Dynamic remodeling of TRPC5 channel–caveolin-1–eNOS protein assembly potentiates the positive feedback interaction between Ca²⁺ and NO signals

Reiko Sakaguchi[1,2,3], Nobuaki Takahashi[1,4], Takashi Yoshida[1,5], Nozomi Ogawa[1], Yoshifumi Ueda[1], Satoshi Hamano[1], Kaori Yamaguchi[6], Seishiro Sawamura[1], Shinichiro Yamamoto[1,5], Yuji Hara[1,7], Tomoya Kawamoto[1], Ryosuke Suzuki[1], Akito Nakao[1], Masayuki X. Mori[1,3], Tetsushi Furukawa[8], Shunichi Shimizu[5], Ryuji Inoue[9], and Yasuo Mori[1,2,4,*]

From the [1]Laboratory of Molecular Biology, Department of Synthetic Chemistry and Biological Chemistry, Graduate School of Engineering, and [2]Institute for Integrated Cell-Material Sciences, Kyoto University, Kyoto, Japan; [3]Laboratory of Biomaterials and Chemistry, School of Medicine, University of Occupational and Environmental Health, Fukuoka, Japan; [4]Advanced Biomedical Engineering Research Unit, Kyoto University, Kyoto, Japan; [5]Division of Pharmacology, Faculty of Pharmaceutical Sciences, Teikyo Heisei University, Tokyo, Japan; [6]Laboratory of Environmental Systems Biology, Department of Technology and Ecology, Hall of Global Environmental Studies, Kyoto University, Kyoto, Japan; [7]Department of Integrative Physiology, School of Pharmaceutical Sciences, University of Shizuoka, Shizuoka, Japan; [8]Department of Bio-informational Pharmacology, Medical Research Institute, Tokyo Medical and Dental University, Tokyo, Japan; [9]Department of Physiology, Fukuoka University, Fukuoka, Japan

Reviewed by members of the JBC Editorial Board. Edited by Mike Shipston

The cell signaling molecules nitric oxide (NO) and Ca²⁺ regulate diverse biological processes through their closely co-ordinated activities directed by signaling protein complexes. However, it remains unclear how dynamically the multicomponent protein assemblies behave within the signaling complexes upon the interplay between NO and Ca²⁺ signals. Here we demonstrate that TRPC5 channels activated by the stimulation of G-protein–coupled ATP receptors mediate Ca²⁺ influx, that triggers NO production from endothelial NO synthase (eNOS), inducing secondary activation of TRPC5 via cysteine S-nitrosylation and eNOS in vascular endothelial cells. Mutations in the caveolin-1–binding domains of TRPC5 disrupt its association with caveolin-1 and impair Ca²⁺ influx and NO production, suggesting that caveolin-1 serves primarily as the scaffold for TRPC5 and eNOS to assemble into the signal complex. Interestingly, during ATP receptor activation, eNOS is dissociated from caveolin-1 and in turn directly associates with TRPC5, which accumulates at the plasma membrane dependently on Ca²⁺ influx and calmodulin. This protein reassembly likely results in a relief of eNOS from the inhibitory action of caveolin-1 and an enhanced TRPC5 S-nitrosylation by eNOS localized in the proximity, thereby facilitating the secondary activation of Ca²⁺ influx and NO production. In isolated rat aorta, vasodilation induced by acetylcholine was significantly suppressed by the TRPC5 inhibitor AC1903. Thus, our study provides evidence that dynamic remodeling of the protein assemblies among TRPC5, eNOS, caveolin-1, and calmodulin determines the ensemble of Ca²⁺ mobilization and NO production in vascular endothelial cells.

"Canonical" transient receptor potential (TRPC) proteins are a subfamily of mammalian TRP protein homologs that bear the highest structural and functional similarity to the founding *Drosophila melanogaster* TRP (1, 2). Being different from members of other TRP subgroups such as TRPV1, TRPA1, and TRPM8, which primarily act as biosensors of extrinsic stress factors, TRPCs are generally recognized as Ca²⁺-permeable cation channels that are closely integrated into the intrinsic signaling cascade comprised of metabotropic receptor activation, phosphatidylinositol 4,5-bisphosphate breakdown by phospholipase C (PLC), and Ca²⁺ mobilization (3). This functional characteristics of TRPCs is represented by their ability to interact with intracellular signaling proteins, comparable to the *Drosophila* TRP that forms a protein assembly essential for the photoreceptor signal transduction (4). For instance, the TRPC3 channel, which is activated by diacylglycerol (5), provides PLCγ2 and protein kinase Cβ with a scaffolding platform at the plasma membrane (6–9). TRPC4 and TRPC5 as well as PLCβ1 and PLCβ2 interact with Na⁺/H⁺ exchanger regulatory factor proteins (10), and dissociation from Na⁺/H⁺ exchanger regulatory factor confers DAG-sensitive state on TRPC4 and TRPC5 channels (11). TRPC1 and TRPC4 also interact with caveolin-1 (12); caveolin-1 retains TRPC1 within the plasma membrane regions nearby STIM1 puncta, enabling TRPC1 to interact with STIM1 and to induce store-operated Ca²⁺ influx (12). In terms of TRPC1 and TRPC6, an association of calmodulin (CaM) has been shown to regulate the Ca²⁺-dependent inactivation (13). Thus, there are ample studies reporting that pre-associated proteins play critical roles in stability, subcellular localization, and functional regulation of TRPC channels. Nevertheless, it remains elusive as to how component proteins are assembled or disassembled within TRPC signaling complexes in response to receptor

stimulation and how this assembly "dynamics" impacts the ensemble of transducing signals in eliciting downstream biological responses.

Nitric oxide (NO) is a cell signaling molecule that controls diverse biological processes such as vascular relaxation and neurotransmission (14, 15). The major sources of NO *in vivo* are the three isoforms of NO synthase (NOS). As a regulator of endothelial NOS (eNOS) and neuronal NOS (nNOS) and other signaling proteins such as some Ca^{2+} channels, caveolin-1, the defining protein constituent of caveolae (16), has been implicated (12, 17–20). It is known that caveolin-1 concentrates signaling molecules within caveolae *via* the binding of its "scaffolding domain" and allows their rapid activation by posttranslational protein modifications and fine-tunes physiological responses (12, 18–22). Also, there is a growing awareness that cysteine *S*-nitrosylation as a posttranslational protein modification is regulated with precise temporal and spatial characteristics (15) and confers specificity to NO-derived effects. Interestingly, protein-protein trans-nitrosylation, the transfer of the NO group between proximal proteins in the absence of apparent NO release, has been proposed as a mechanism conferring to *S*-nitrosylation a targeting specificity (23, 24). These specific and regulated functions of *S*-nitrosylation contrast with the global control of redox state and allow *S*-nitrosylation to convey redox-based cellular signals (15).

NO signaling is precisely coordinated with Ca^{2+} signaling in at least two ways (25). Most importantly, an increase in intracellular Ca^{2+} concentration ($[Ca^{2+}]_i$) activates the Ca^{2+}-dependent NOS isoforms eNOS and nNOS (26). In endothelial cells, eNOS is maintained in its inactive state through association with caveolin-1. Upon $[Ca^{2+}]_i$ elevation, which can be induced by Ca^{2+} entry across the plasma membrane and Ca^{2+} release from ER, eNOS forms a complex with CaM and dissociates from caveolin-1, thereby increasing its NO-producing enzymatic activity (27). Multiple Ca^{2+} entry channels including TRPC1/C4/C5 and TRPV4 are known to be expressed in endothelial cells (28, 29). However, it is still unclear whether activation of eNOS requires specific modes or machineries of upstream Ca^{2+} mobilization (30–33), in contrast with nNOS, whose activation by Ca^{2+} influx through N-methyl-D-aspartate receptors (NMDARs) in neurons is well documented (15, 34). Another important aspect of NO-Ca^{2+} coordination is feedback regulation of Ca^{2+} mobilization by the cysteine *S*-nitrosylation on receptors and channels, which controls $[Ca^{2+}]_i$ (25). This remains a contentious issue in endothelial cells (35): both positive (36, 37) and negative (38, 39) regulation of Ca^{2+} mobilization pathways by NO have been reported. In neurons, NO produced by nNOS causes cysteine *S*-nitrosylation of NMDARs and decreases their Ca^{2+} influx activity (15, 40, 41), while in cardiac myocytes, the ryanodine receptor 2 is *S*-nitrosylated by the muscle-specific nNOS variant (42, 43), which associates with ryanodine receptor 2 at the sarcoplasmic reticulum (15, 44) and enhances Ca^{2+} release activity (15, 42). However, such feedback processes *via S*-nitrosylation are yet to be clarified in other cell types including endothelial cells. Thus, the molecular identification of eNOS-activating Ca^{2+}

mobilization machinery as well as its *S*-nitrosylation–mediated feedback regulation are major questions to be addressed in understanding NO-Ca^{2+} signal coordination.

We have previously found that the number of TRPC channels including TRPC5 are activated by NO through cysteine *S*-nitrosylation (24, 45–47). We also showed that in bovine aortic endothelial cells (BAECs), TRPC5 is colocalized with eNOS and is activated by NO produced by eNOS upon stimulation of G-protein–coupled ATP receptor–mediated Ca^{2+} entry (46). TRPC5 and eNOS are thus likely to be the key to delineating the interplay between Ca^{2+} and NO signaling pathways in vascular endothelial cells, which compelled us to investigate the precise dynamics of physical and functional interaction between TRPC5 and eNOS. In this study, we reveal that receptor activation initiates TRPC5-mediated Ca^{2+} influx and triggers NO production by eNOS, which leads to subsequent secondary activation of TRPC5 *via* cysteine *S*-nitrosylation in BAECs. Interestingly, caveolin-1 can act as a protein scaffold for eNOS and TRPC5, regulating the assembly of TRPC5 and eNOS in a Ca^{2+}/CaM-dependent manner. These studies suggest that a dynamic quadripartite interaction of TRPC5, eNOS, caveolin-1, and CaM finely tunes receptor-activated NO and Ca^{2+} signaling. This study would also shed light to the controversy regarding the direct regulation of TRPC5 by NO (24, 46, 48–50).

Results

eNOS function is critical for vasodilator-induced Ca^{2+} elevation in endothelial cells

We first evaluated the Ca^{2+} response and NO production by applying the vasodilator ATP, which activates P2Y and triggers $[Ca^{2+}]_i$ elevation and eNOS-mediated NO production in endothelial cells (32, 46). Upon ATP stimulation in BAECs, continuous $[Ca^{2+}]_i$ elevation occurred, which was partially (32%) suppressed by siRNA treatment specific to eNOS (sieNOS) (Figs. 1*A* and S1*A*). The NOS inhibitor N^{ω}-nitro-L-arginine methylester (L-NAME) nearly abrogated (by 69%) NO production in BAECs visualized by NO indicator DAF-2 (Fig. 1*B*), but eNOS inhibition by sieNOS (46) only partially (34%) suppressed the Ca^{2+} influx (Fig. 1*C*).

eNOS is functionally coupled with TRPC5 channels *via* NO production in endothelial cells

We next searched for the molecule responsible for this Ca^{2+} influx. We have previously shown that TRPC5 is activated by NO through cysteine *S*-nitrosylation and is colocalized with eNOS which can activate TRPC5 by NO produced upon stimulation of G-protein–coupled ATP receptor–mediated Ca^{2+} entry (46). Here, we further examined the subcellular distribution of endogenous TRPC5. Immunocytochemistry showed colocalization of TRPC5 with eNOS near the plasma membrane in BAECs (Fig. 1*D*). Proximity ligation assay (PLA), which allows the detection of protein–protein interactions at distances less than 40 nm (51), also confirmed that TRPC5 and eNOS are in a close vicinity in BAEC endogenously expressing these two molecules (Fig. 1*E*). Furthermore, eNOS co-
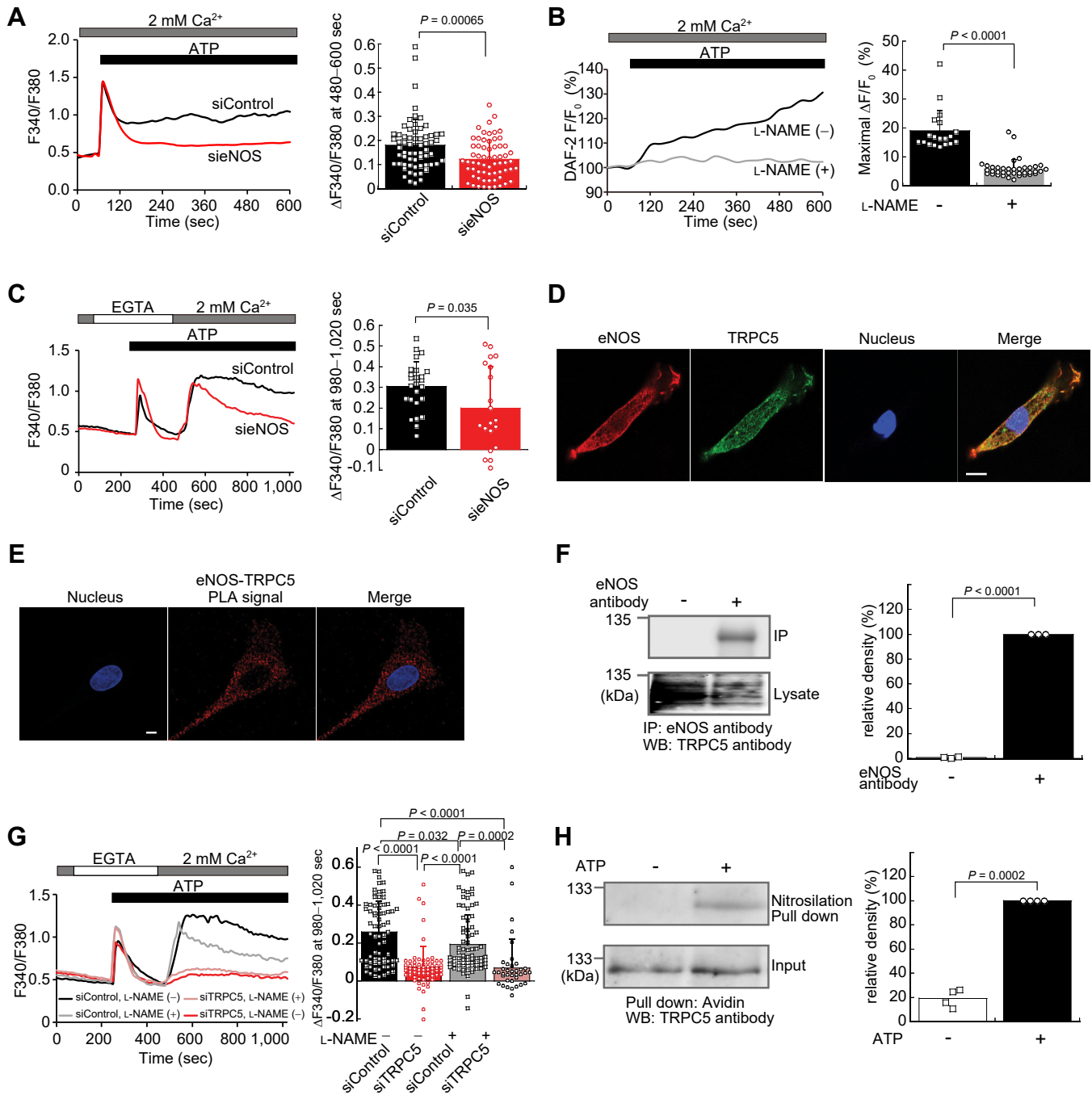
Figure 1. Physical and functional coupling of native TRPC5 proteins associated with eNOS in BAECs. *A*, $[Ca^{2+}]_i$ increases (340:380-nm fluorescence ratio; F340/F380) in sieNOS- or siControl-transfected BAECs in response to ATP. Representative time courses (*left*) and averaged $[Ca^{2+}]_i$ increases during 480 to 600 s (*right*) (*n* = 64 each). The averaged ratio during 10 to 50 s was subtracted as background for each of the cells to derive ΔF340/F380. *B*, intracellular NO production evoked by 1 μM ATP in BAECs treated with or without 10 μM L-NAME. Representative time courses of DAF-2 fluorescent changes (F/F₀) (*left*) and maximal fluorescent increases (ΔF/F₀) (*right*) (*n* = 19–38). *C*, $[Ca^{2+}]_i$ increases in sieNOS- or siControl-transfected BAECs in 0.5 mM EGTA (Ca²⁺-free)- or 2 mM Ca²⁺-containing solution. Representative time courses (*left*) and averaged $[Ca^{2+}]_i$ increases during 980–1020 s (*right*) (*n* = 20–25). In *A* to *C*, 3 mM L-arginine is added to the bath solutions. *D*, confocal fluorescence images of protein localization in BAECs. Specific antibodies are used to detect TRPC5 (*green*) and eNOS (*red*). The nuclei are stained with Hoechst 33342 (*blue*). The bar indicates 10 μm. *E*, confocal fluorescence images of TRPC5-eNOS colocalization in BAEC visualized by proximity ligation assay (PLA). Specific antibodies for TRPC5 and eNOS were used to obtain PLA signal (*red*). The nuclei are stained with DAPI (*blue*). The bar indicates 5 μm. *F*, co-immunoprecipitation of TRPC5 with eNOS in BAEC. Immunoprecipitates (IPs) with or without anti-eNOS antibody are subjected to western blotting (WB) with antibody to TRPC5 (*left*). *Right*, quantification of gel image. *G*, $[Ca^{2+}]_i$ increases evoked by 1 μM ATP in 0.5 mM EGTA- or 2 mM Ca²⁺-containing solution, in siTRPC5- or siControl-transfected BAECs treated with or without 10 μM L-NAME. Representative time courses (*left*) and averaged $[Ca^{2+}]_i$ increases (ΔF340/F380) during 980–1020 s (*right*) (*n* = 38–78). *p* values are determined by one-way ANOVA with subsequent paired comparison. *H*, *S*-nitrosylation assay (biotin switch assay) of TRPC5 in BAECs. The cells are treated with 1 μM ATP for 5 min. The collected cell lysates are treated with biotin-HPDP to selectively label *S*-nitrosylated proteins (*left*). *Right*, quantification of gel image. For *A*, *B*, *C*, and *G*, individual data points indicate individual cells examined, and for all the gel images, individual data points indicate technical replicates. Data points are mean ± SD.

immunoprecipitated with TRPC5 in BAEC (Fig. 1F), supporting the physical coupling of the two molecules.

We next examined the possible functional coupling of TRPC5 and eNOS. ATP stimulation in BAECs induced $[Ca^{2+}]_i$ elevation *via* a combination of Ca^{2+} release from intracellular stores (shown in the absence of extracellular Ca^{2+}) and Ca^{2+} influx (apparent following the re-introduction of extracellular Ca^{2+}) (Fig. 1G, black trace). TRPC5-targeted siRNA (siTRPC5, Fig. S1B) (46) had a severe diminishing effect (65–71%) on the Ca^{2+} influx by suppressing both the L-NAME–sensitive and L-NAME–insensitive components (Fig. 1G), suggesting that Ca^{2+} influx *via* TRPC5 in BAECs contributes to eNOS-dependent and eNOS-independent components of ATP receptor–activated $[Ca^{2+}]_i$ elevation. Importantly, *S*-nitrosylation of TRPC5 proteins in BAECs was induced by ATP receptor stimulation (Fig. 1H). Given that our previous report showed that TRPC5 was resistant to ODQ, the downstream pathway of NO signal that produces cGMP is unlikely to be involved. Therefore, we think it is very likely that NO is directly activating TRPC5 by *S*-nitrosylation to induce secondary Ca^{2+} influx. These lines of evidence suggest that upon receptor stimulation in endothelial cells, Ca^{2+} influx *via* receptor-activated TRPC5 channels elicits NO production by eNOS, which may in turn induce secondary activation of Ca^{2+} influx *via* cysteine *S*-nitrosylation of TRPC5.

Subtype-selectivity of TRPC coupling to eNOS

We next examined the interaction between TRPC subtypes and eNOS using a heterologous expression system in human embryonic kidney 293 cells. We took advantage of using HEK293 cell line because it expresses P2Y receptors almost exclusively (45), making it possible to examine the sole effect of ATP stimulation. As seen in BAECs, TRPC5-DsRed was colocalized with eNOS-GFP in the plasma membrane (82%; Fig. 2A). This is consistent with the results from PLA, also indicating that the two molecules are in a close vicinity (Fig. 2B).

Co-expression of eNOS enhanced ATP receptor–activated Ca^{2+} influx in HEK293 cells expressing TRPC5 by 2.0-fold but not in those expressing other TRPC subtypes; Ca^{2+} response of TRPC4 was also increased by eNOS co-expression by 4.6-fold, although this effect was not statistically significant (Fig. 2C and 2D). In addition, eNOS-GFP co-immunoprecipitated with TRPC5-Flag, but not with TRPC3-Flag (Fig. 2E). The enhanced Ca^{2+} influx *via* TRPC5 was substantially suppressed to 47% by L-NAME (Fig. 2F), indicating the NO-dependence of this phenomenon, consistent with the observation that co-expression of TRPC5 with eNOS elicited NO production upon receptor stimulation (Fig. 2G). In addition, receptor-stimulated *S*-nitrosylation of TRPC5 was observed in HEK293 cells expressing eNOS (Fig. 2H).

In TRPC5-expressing HEK293 cells using whole-cell patch clamp recording, we confirmed that ATP-induced whole-cell currents had a typical "N-shaped" current-voltage (*I-V*) relationship (Fig. 2I), which corresponds well with those reported previously for TRPC5 (45, 46). ATP-activated TRPC5 currents

were consistently enhanced to 5.3-fold by co-expression of eNOS (Fig. 2, I and J). These results suggest that, among the TRPC isoforms, TRPC5 preferentially interacts with eNOS to promote Ca^{2+} and NO signaling pathways.

Caveolin-1 provides a scaffold for complexing of TRPC5 and eNOS

Caveolin-1 is a scaffolding protein that negatively regulates eNOS activity through direct association (27). We therefore examined contribution of caveolin-1 to the formation of TRPC5–eNOS complex. Physical interaction of TRPC5 with caveolin-1 was validated both by immunocytochemistry and co-immunoprecipitation in BAEC (Fig. 3, A and B). Co-immunoprecipitation using extracts from HEK293 cells expressing GFP-labeled TRPC5 (TRPC5-GFP) and Flag-tagged caveolin-1 (caveolin-1-Flag) also confirmed the interaction between these molecules (Fig. 3C). It was therefore conceivable that TRPC5 is *S*-nitrosylated by eNOS in a protein complex comprised of TRPC5, eNOS, and caveolin-1. However, as observed in other reports (52), we have found that the endogenous level of caveolin-1 expression was heterogeneous among individual HEK293 cells we used (Fig. S2, A and B), which might obscure the effect of caveolin-1. This issue was addressed by testing the effects of exogenous expression of caveolin-1 in HEK293 cells. Caveolin-1 overexpression moderately suppressed the enhancement by eNOS of TRPC5-mediated Ca^{2+} influx (20%) and eNOS-mediated NO production (48%) upon receptor stimulation (Fig. S2, C and D), consistent with the previous reports suggesting the role of caveolin-1 as a negative regulator of eNOS (14). The overexpression of caveolin-1 did not alter the localization of eNOS or TRPC5, when compared with control cells only expressing endogenous caveolin-1 (Figs. 2A and S2E), as suggested in previous reports (53, 54). These data indicate that caveolin-1 at the endogenous level provides a sufficient scaffold for TRPC5-eNOS coupling in HEK293 cells.

To analyze the molecular interaction of TRPC5 with caveolin-1, we assessed the *in vitro* binding of TRPC5 fragments to caveolin-1 in a glutathione *S*-transferase (GST) pull-down assay (Figs. 3, D and E, and S3). When the extract from HEK293 cells expressing caveolin-1-GFP was incubated with glutathione-Sepharose beads bound to TRPC5-GST fragments, the TRPC5 N-terminal residues 1 to 330 showed strong binding to caveolin-1-GFP, whereas residues 625 to 975 showed only weak (27%) interaction and residues 352 to 398 exhibited essentially no detectable interaction (Fig. 3E). This indicates that the N-terminal cytoplasmic region of TRPC5 (residues 1–330) carries the major binding region for caveolin-1. Notably, two putative caveolin-binding motifs, residues 6 to 14 and residues 295 to 322, are present in the N-terminal cytoplasmic region of TRPC5 (Fig. 3D) (17, 55, 56). Three-dimensional structure revealed that residues 6 to 14 are in a disordered region, but residues 295 to 322 are located just below the transmembrane region (Fig. 3F). This amino acid sequence
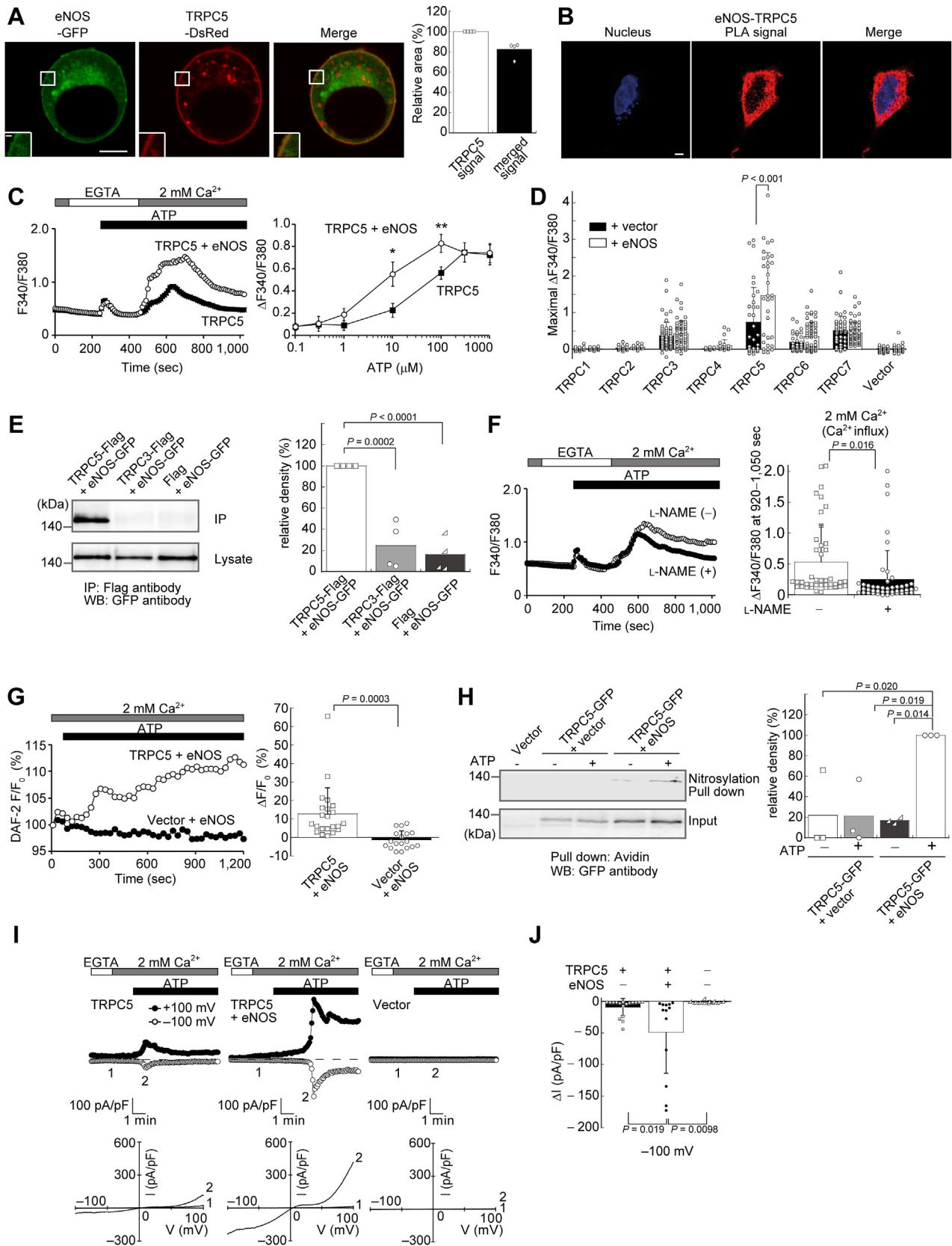
Figure 2. TRPC subtype-selectivity of functional coupling with eNOS in HEK293 cells. *A*, confocal fluorescent images of HEK293 cells expressing eNOS-GFP and TRPC5-DsRed. The bar indicates 5 μm. The insets show enlarged views of the boxed regions (*left*). The bar indicates 0.5 μm. *Right*, quantification of the area exhibiting merged signal relative to the area exhibiting TRPC5 signal. *B*, confocal fluorescence images of TRPC5-eNOS colocalization in HEK293 visualized by PLA. Specific antibodies for TRPC5 and eNOS were used to obtain PLA signal (*red*). The nuclei are stained with DAPI (*blue*). The bar indicates 5 μm. *C*, [Ca^{2+}]$_i$ increases evoked by ATP in 0.5 mM EGTA- or 2 mM Ca^{2+}-containing solution, in TRPC5-expressing HEK293 cells cotransfected with vector or

(295–322) is well conserved among the TRPC subfamily (Fig. 3*G*) and the corresponding sequence has previously been proposed as a major caveolin-binding domain for TRPC1 (55). We used co-immunoprecipitation assays to evaluate the association of each of these domains and their constructs with mutations that abolish protein interaction (TRPC5$_{Y6A/Y11A/Y14A}$ and TRPC5$_{Y296A/F301A}$) with caveolin-1 (57). The association between caveolin-1 and TRPC5 was absent for the TRPC5$_{Y296A/F301A}$ mutant but was maintained in the TRPC5$_{Y6A/Y11A/Y14A}$ mutant (Fig. 3*H*), suggesting that residues 295 to 322 of TRPC5 form the major binding domain for caveolin-1 in TRPC5.

Caveolin-1 binding is essential for functional coupling of TRPC5 and eNOS

We next explored the caveolin-1 dependence of the interaction between eNOS and TRPC5 using TRPC5$_{Y296A/F301A}$. The association with eNOS and the potentiating effect of eNOS on Ca^{2+} influx *via* TRPC5 were both abrogated in the TRPC5$_{Y296A/F301A}$ mutant (Fig. 4, *A* and *B*) compared with the intact TRPC5 (Fig. 4*A*, dashed line), suggesting that TRPC5 forms a protein complex with eNOS *via* caveolin-1. The Y296A/F301A mutation also decreased the total colocalization of TRPC5 with eNOS from 82% (Fig. 2*A*) to 56% (Fig. 4*C*). Colocalization of the TRPC5 mutant and eNOS was mainly observed in the inner membrane. In a similar context, a mutant eNOS with changes in the caveolin-binding motif (eNOS-MutCBD) had impaired association (10%) with caveolin-1 (Fig. 4*D*). Association with TRPC5 and enhancement of TRPC5-mediated Ca^{2+} influx upon receptor stimulation were both abrogated (down to 23% and 66%, respectively) in the eNOS-MutCBD mutant (Fig. 4, *E* and *F*). Furthermore, the importance of caveolin-1 binding in the enhancement of Ca^{2+} influx by eNOS was also confirmed in BAECs treated with siRNA targeted to caveolin-1 (Fig. 4*G*). These data strongly support our hypothesis that caveolin-1 provides the scaffold for TRPC5 and eNOS to assemble into a signaling complex to regulate NO and Ca^{2+} signaling. In agreement with this notion, the caveolin-1-Flag construct was co-immunoprecipitated with both TRPC5-GFP and eNOS-GFP (Fig. S4), and the TRPC5-Flag construct was co-immunoprecipitated with both caveolin-1-GFP and eNOS-GFP (Fig. S4), when co-expressed in HEK293 cells.

TRPC5–eNOS complex is dynamically remodeled by [Ca^{2+}]i elevation during receptor stimulation

The data above prompted us to examine the dynamic properties of the association between TRPC5 and eNOS. We monitored the TRPC5–eNOS complex formation by fluorescence resonance energy transfer (FRET) measurements. In the presence of extracellular Ca^{2+}, the FRET/CFP ratios in the plasma membrane were enhanced by ATP receptor stimulation in HEK293 cells co-expressing TRPC5-CFP and eNOS-YFP (Fig. 5, *A* and *B*). Population-based evaluation by surface labeling assay revealed the ATP-dependent accumulation of TRPC5 and eNOS in the plasma membrane, which also agrees well with the FRET analysis (Fig. S5*A*).

Similar to this notion, stimulation of ATP receptor induced 1.6-fold increase of the level of co-immunoprecipitation of TRPC5-Flag with eNOS-GFP in a time-dependent manner (Fig. 5, *C* and *D*) in HEK293 cells. This increase of receptor-driven association was not statistically significant. However, the omission of extracellular Ca^{2+} significantly suppressed the increase of association, revealing the importance of TRPC5-mediated Ca^{2+} influx. (1 min; Fig. 5, *C* and *D*). For comparison, under the presence of overexpressed caveolin-1, stimulation of ATP receptor increased the co-immunoprecipitation of TRPC5-Flag with eNOS-GFP in a time-dependent manner, but the binding fraction was suppressed during the early phase (time period 1–5 min) of ATP stimulation (Fig. S5, *B* and *C*). It is known that CaM responsible for the activation of eNOS binds to eNOS only after the formation of Ca^{2+}-CaM, but not in the apo form (58, 59). The CaM mutant (CaM-Mut), rendered insensitive to Ca^{2+} by mutation in all four EF-hand domains (60), therefore would not bind to the activation site of eNOS even when [Ca^{2+}]$_i$ is elevated. Notably, overexpression of CaM-Mut altered the effect of receptor-driven association (Fig. 5*E*). In line with this observation, co-expression of CaM-Mut abolished eNOS-(NO-) dependent component of Ca^{2+} influx *via* *S*-nitrosylated-TRPC5 (Fig. 5*F*). Together, these findings suggest that [Ca^{2+}]$_i$ elevation by Ca^{2+} influx positively regulates the formation of TRPC5–eNOS complexes *via* Ca^{2+}-CaM. Interestingly, the overexpression of CaM-Mut resulted in the constant association between eNOS and TRPC5 (Fig. 5*E*). At the basal state of native HEK293 cells, certain protein(s) different from eNOS may be already associated with endogenous apo CaM, which

---

eNOS. Averaged time courses (*left*) and dose-response relationships of maximal [Ca^{2+}]$_i$ increases in 2 mM Ca^{2+}-containing solution (*right*) (*n* = 33–34). **p* < 0.05 and ***p* < 0.01, as compared to the cells cotransfected with TRPC5 and vector. *D*, maximal [Ca^{2+}]$_i$ increases evoked by 100 μM ATP in 2 mM Ca^{2+}-containing solution in TRPC homolog-expressing HEK293 cells cotransfected with vector or eNOS (*n* = 13–68). *p* values determined by two-way ANOVA with subsequent paired comparison. *E*, co-immunoprecipitation of eNOS-GFP occurs with TRPC5-Flag but not with TRPC3-Flag. IPs with Flag-specific antibody are subjected to WB with antibody to GFP (*left*). *Right*, quantification of gel image. *p* values are determined by one-way ANOVA with subsequent paired comparison. *F*, [Ca^{2+}]$_i$ increases evoked by 100 μM ATP in 0.5 mM EGTA- or 2 mM Ca^{2+}-containing solution, in TRPC5- and eNOS-expressing HEK293 cells treated with or without 300 μM L-NAME. Averaged time courses (*left*) and averaged [Ca^{2+}]$_i$ increases during 920–1050 s in Ca^{2+}-containing solution (*right*) (*n* = 42–45). *G*, DAF-2 fluorescent changes evoked by 1 mM ATP in eNOS-expressing HEK293 cells cotransfected with vector or TRPC5. Averaged time courses (F/F$_0$) (*left*) and averaged fluorescent increases during 1080–1200 s (ΔF/F$_0$) (*right*) (*n* = 18–23). In C, D, F, and G, 3 mM L-arginine is added to the bath solutions. *H*, *S*-nitrosylation assay in HEK293 cells. Cells cotransfected with TRPC5-GFP and eNOS constructs are treated with or without 100 μM ATP for 10 min. The collected cell lysates are treated with biotin-HPDP to selectively label *S*-nitrosylated proteins (*left*). *Right*, quantification of gel image. *p* values are determined by one-way ANOVA with subsequent paired comparison. *I*, representative time courses of 100 μM ATP-evoked outward and inward whole cell currents under ramp clamp conditions, in TRPC5-expressing HEK293 cells cotransfected with eNOS construct. The corresponding *I-V* relationships at time points 1 and 2 are also shown. *J*, ATP-evoked current responses (Δ*I*) of TRPC5 at −100 mV (n = 11–17). *p* values are determined by one-way ANOVA with subsequent paired comparison. Three mM L-arginine is added to the bath solutions. For *D*, *F*, *G*, and *J*, individual data points indicate individual cells examined, and for all the gel images, individual data points indicate technical replicates. Data points are mean ± SD.
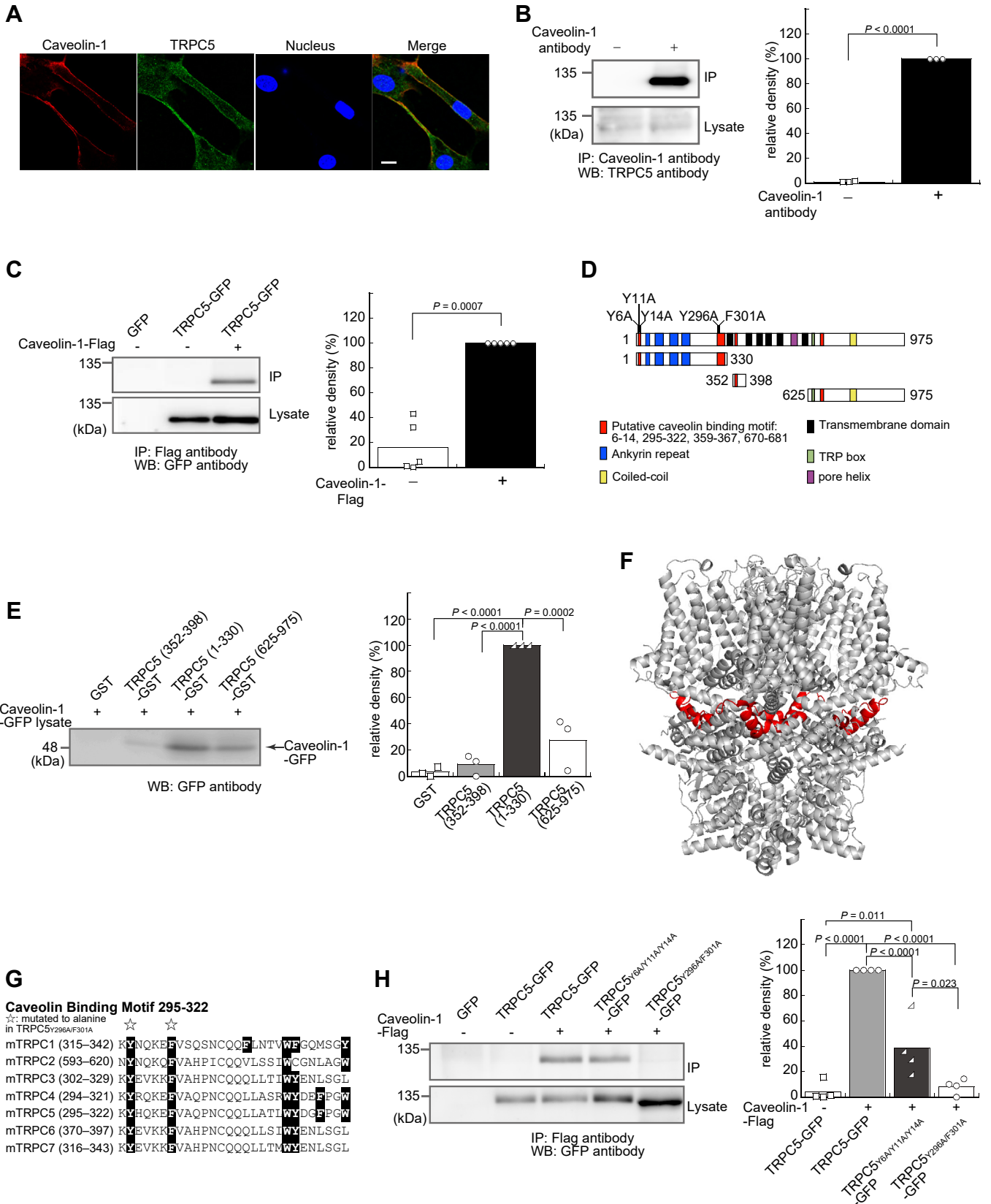
Figure 3. Caveolin-1 binds to the C-terminus of TRPC5 to form a complex. *A*, confocal fluorescence images of protein localization in BAECs. Specific antibodies are used to detect TRPC5 (*green*) and caveolin-1 proteins (*red*). The nuclei are stained with Hoechst 33342 (*blue*). The bar indicates 10 μm. *B*, co-immunoprecipitation of TRPC5 with caveolin-1 in BAEC. IPs with anti-caveolin-1 antibody are subjected to WB with antibody to TRPC5 (*left*). *Right*, quantification of gel image. *C*, co-immunoprecipitation of TRPC5-GFP with caveolin-1-Flag in HEK293 cells. IPs with Flag-specific antibody are subjected to WB with antibody to GFP (*left*). *Right*, quantification of gel image. *D*, a schematic representation of GST fusion proteins of mouse TRPC5 subfragments. *E*, pull

binds to entered Ca^{2+} to trigger the plasma membrane targeting of eNOS for subsequent association with TRPC5.

On the other hand, association of eNOS with activated CaM is known to be competitive to caveolin-1 binding. Therefore, increase of $[Ca^{2+}]_i$ could induce the dissociation of eNOS from TRPC5 *via* caveolin-1. We tested the effect of Ca^{2+} concentration to eNOS–TRPC5 complex formation. GST pull-down assays using extracts from HEK293 cells expressing recombinant eNOS-GFP and CaM as well as endogenous caveolin-1 showed that the N-terminal fragment of TRPC5 containing the residues 1 to 330 (and thus the caveolin-binding domain at residues 295–322) bound exclusively to eNOS in a buffer containing Ca^{2+} at a low concentration (100 nM) (Fig. 5G). In contrast, when the same experiment was performed at a physiologically high Ca^{2+} concentration (10 µM) mimicking the $[Ca^{2+}]_i$ elevation after ATP stimulation, the C-terminal fragment of TRPC5 (residues 625–975) bound extensively to eNOS (Fig. 5H). This result suggests that eNOS, which forms a complex indirectly with TRPC5 *via* caveolin-1 at low $[Ca^{2+}]_i$ (100 nM) (Fig. 5G), is released from caveolin-1 to directly interact with the C-terminal region of TRPC5 at high $[Ca^{2+}]_i$ (10 µM) (Fig. 5H). Docking simulation using AlphaFold 2 algorithm (61, 62) predicted a reasonable direct interaction between eNOS and C-terminal region of TRPC5 (residues 936–975) (Fig. S6, A and B), in a good agreement with the GST pull-down assay (Fig. 5H). The direct interaction site of eNOS was further explored by using TRPC5 variants lacking this region. GST pull-down assay revealed that the interaction between eNOS and TRPC5 was significantly suppressed when the C terminus residues 955 to 975 are truncated, strongly suggesting that this region is critical for eNOS binding (Fig. S6E). This Ca^{2+}-dependent shift of protein interaction site on TRPC5 may enable eNOS to produce NO in the vicinity of TRPC5, enhancing the efficiency of *S*-nitrosylation and secondary activation of TRPC5, which amplifies Ca^{2+} signaling (Fig. 5I).

Spatio-temporal dynamics of the localization of TRPC5–eNOS protein complexes

To further investigate the spatio-temporal distribution of eNOS and TRPC5 following stimulation of the ATP receptor, evanescent wave microscopy was used to illuminate only the subcellular area from the surface of the cell to a depth of less than 100 nm through total internal reflection fluorescence (TIRF). The plasma membrane localization of eNOS-GFP and TRPC5-GFP, expressed alone in HEK293 cells, was respectively decreased (27) and increased (63) immediately after application of ATP (Fig. 6, A–C). In contrast, when eNOS-GFP was co-expressed with TRPC5, the amount of eNOS-GFP near the cell surface was initially decreased and subsequently increased upon ATP stimulation. Importantly, the observed changes in the plasma membrane localization of TRPC5 and eNOS upon receptor stimulation were nearly undetectable when extracellular Ca^{2+} was chelated with EGTA (Fig. 6, D–F). These results suggest that TRPC5-eNOS association is dynamically regulated by Ca^{2+} influx in the plasma membrane upon ATP receptor stimulation. These findings, together with the dynamics visualized by FRET analysis (Fig. 5, A and B), suggest that in addition to the cytosol as reported previously (27), eNOS is translocated also toward TRPC5 in the plasma membrane after dissociation of eNOS from caveolin-1 is induced by $[Ca^{2+}]_i$ elevation.

Pharmacological inhibition of TRPC5 suppresses acetylcholine-induced artery dilation

To confirm our concept, we evaluated the function of TRPC5 in rat artery *ex vivo* taking the advantage of a TRPC5-selective inhibitor AC1903 (64). We chose to take this pharmacological approach considering that TRPC1 and TRPC4 which form heteromers with TRPC5 could compensate TRPC5 gene knock out in endothelial NO production (65, 66). Immuno-histochemistry performed for the whole mount preparation of rat mesenteric artery revealed colocalization of TRPC5 and eNOS in the endothelial cell layer (Fig. 7A). TRPC5 and eNOS were distributed on both the luminal and abluminal sides of the endothelial cell layer of the vascular tissue, along with caveolin-1 (Fig. 7B).

Freshly isolated rat aorta was first contracted by phenylephrine treatment followed by acetylcholine stimulation, which facilitated relaxation of aorta (Fig. 7C). In contrast, when the aorta was pretreated with AC1903, a TRPC5-selective inhibitor (64), this relaxation was significantly suppressed to 62% (Fig. 7, D and E). This result strongly supports the idea that TRPC5 physiologically contributes to the NO-mediated relaxation upon vasodilator stimulation in aorta.

Discussion

In the present study, we show that TRPC5 is physically and functionally associated with eNOS to form a dynamic complex that regulates interplay between NO and Ca^{2+} signaling in vascular endothelial cells (Fig. 8). Within this signaling complex, caveolin-1 serves as a scaffolding protein for eNOS and TRPC5 and suppresses their activities. It is well documented that eNOS binds to caveolin-1 at low Ca^{2+} but dissociates from caveolin-1 at high Ca^{2+} (67–69). Our results suggest that although TRPC5 is not an absolute requirement for this regulation, it accelerates the protein relocation in endothelial cells (Figs. 6B and 8, B–D). Once Ca^{2+} influx *via* TRPC5 is activated through the PLC cascade upon stimulation of ATP receptors, the indirect association of TRPC5 with eNOS *via*

down assay of caveolin-1 with GST fusion proteins of TRPC5 fragments. GST fusion proteins immobilized on glutathione-sepharose beads are incubated with cell lysates obtained from HEK293 cells transfected with caveolin-1-GFP. Bound proteins are analyzed by WB with antibody to GFP (*left*). *Right*, quantification of gel image. *p* values are determined by one-way ANOVA with subsequent paired comparison. *F*, structural analysis of the caveolin-1–binding region of TRPC5. *Red* regions represent the putative caveolin-1–binding motif 295 to 322 (PDBID: 7e4t). *G*, an alignment of the putative caveolin-1–binding domain in the N-terminus for mouse TRPC proteins. *H*, co-immunoprecipitation studies of TRPC5-GFP constructs with caveolin-1-Flag. IPs with Flag-specific antibody are subjected to WB with antibody to GFP (*left*). *Right*, quantification of gel image. *p* values are determined by one-way ANOVA with subsequent paired comparison. Individual data points indicate technical replicates for all the gel images.
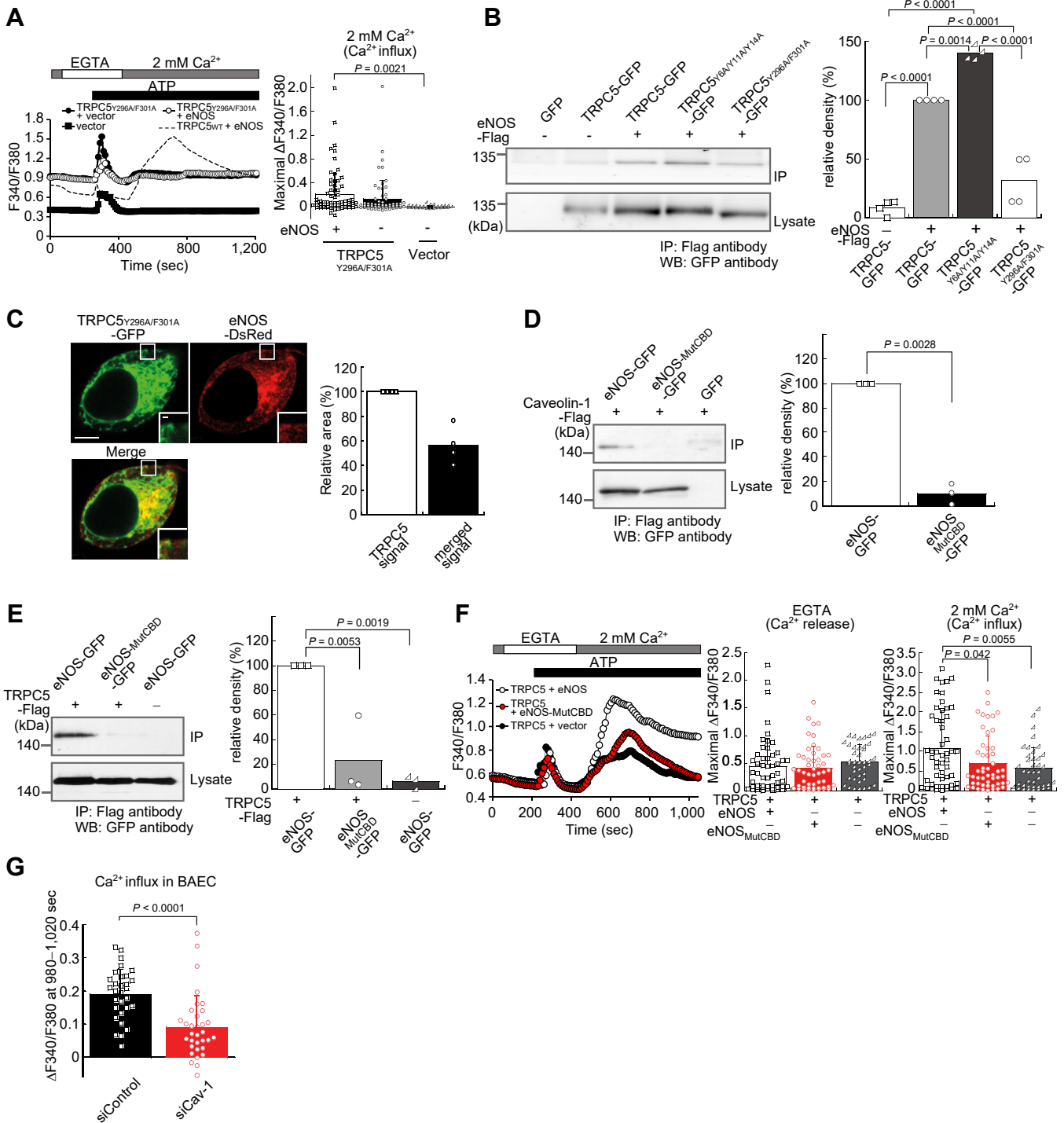
Figure 4. The mutation in the caveolin-1–binding domain of TRPC5 and eNOS abrogates their physical and functional coupling. *A*, $[Ca^{2+}]_i$ increases evoked by 100 μM ATP in 0.5 mM EGTA- or 2 mM Ca^{2+}-containing solution, in TRPC5$_{Y296A/F301A}$-expressing HEK293 cells cotransfected with eNOS or vector. *Dashed* line indicates the result obtained from WT TRPC5 cotransfected with eNOS in a separate experiment for comparison. Averaged time courses (*left*) and maximal $[Ca^{2+}]_i$ increases in Ca^{2+}-containing solution (*right*) (n = 39–72). *p* values are determined by one-way ANOVA with subsequent paired comparison. Three millimolars of L-arginine is added to the bath solutions. *B*, co-immunoprecipitation studies of TRPC5-GFP constructs with eNOS-Flag. IPs with Flag-specific antibody are subjected to WB with antibody to GFP (*left*). *Right*, quantification of gel image. *p* values are determined by one-way ANOVA with subsequent paired comparison. *C*, confocal fluorescent images of HEK293 cells expressing TRPC5$_{Y296A/F301A}$-GFP and eNOS-DsRed. The bar indicates 5 μm. The insets show enlarged views of the boxed regions (*left*). The bar indicates 0.5 μm. *Right*, quantification of the area exhibiting merged signal relative to the area exhibiting TRPC5$_{Y296A/F301A}$ signal. *D*, co-immunoprecipitation studies of eNOS-GFP constructs with caveolin-1-Flag (*left*). *Right*, quantification of gel image. *E*, co-immunoprecipitation studies of eNOS-GFP constructs with TRPC5-Flag (*left*). *Right*, quantification of gel image. *p* values are determined by one-way ANOVA with subsequent paired comparison. *F*, $[Ca^{2+}]_i$ increases evoked by 100 μM ATP in 0.5 mM EGTA- or 2 mM Ca^{2+}-containing solution, in TRPC5-expressing HEK293 cells cotransfected with eNOS constructs. Averaged time courses (*left*) and maximal $[Ca^{2+}]_i$ increases (ΔF340/F380) in EGTA- or Ca^{2+}-containing solution (*right*) (n = 40–52). *p* values are determined by one-way ANOVA with subsequent paired comparison. *G*, $[Ca^{2+}]_i$ increases of siCaveolin-1- or siControl-transfected BAECs in 2 mM Ca^{2+}-containing solution evoked by 100 μM ATP. Averaged $[Ca^{2+}]_i$ increases (ΔF340/F380) during 980–1020 s are shown (n = 32–33). For *A*, *F*, and *G*, individual data points indicate individual cells examined, and for all the gel images, individual data points indicate technical replicates. Data points are mean ± SD.
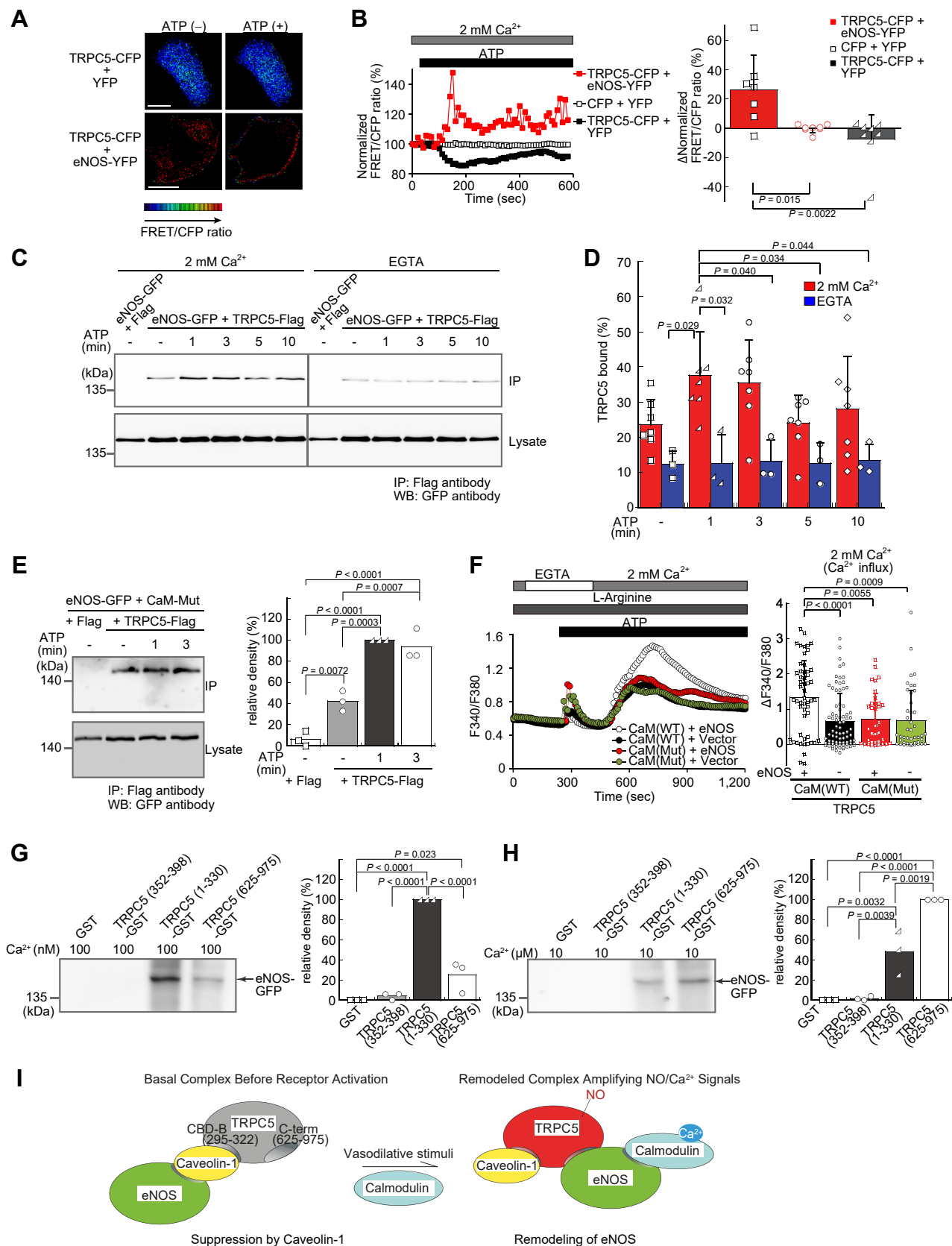
Figure 5. Formation of TRPC5–eNOS complexes is enhanced and remodeled by [Ca²⁺]ᵢ elevation during receptor stimulation. *A,* representative FRET/CFP ratio images (pseudo-color) of HEK293 cells co-expressing TRPC5-CFP and YFP or TRPC5-CFP and eNOS-YFP upon treatment with or without 100 μM ATP in 2 mM Ca²⁺-containing solution. The bars indicate 10 μm. *B,* averaged time courses (*left*) of the normalized FRET/CFP ratio in the plasma membrane area of HEK293 cells co-expressing TRPC5-CFP with eNOS-YFP, CFP with YFP, or TRPC5-CFP with YFP upon treatment with 100 μM ATP in 2 mM Ca²⁺-containing solution (*n* = 7–8). Data are presented as the FRET/CFP ratio normalized to that at *t* = 0. Averaged increases (*right*) in normalized FRET/CFP ratio

caveolin-1 is remodeled into a direct association; eNOS released by the binding action of Ca^{2+}-CaM from caveolin-1 interacts with the C terminus of TRPC5 (residues 625–975), possibly residues 936 to 975 revealed by computational analysis and GST pull-down assay, which is not conserved among other TRPCs and thus specific to TRPC4 and TRPC5 (Figs. 5H and S6, E and F). This region is disordered in the reported 3-dimensional structure resolved by cryo-EM (56), possibly because it can form a helix and stabilize by eNOS interaction. This interaction allows eNOS to produce NO in the vicinity of TRPC5 at the plasma membrane, enhancing secondary activation of TRPC5 through S-nitrosylation and consequent Ca^{2+} signaling, resulting in effective vasodilation (Fig. 8D). Although we have previously reported that P2Y receptors mediate the activation of TRPC5 channels *via* G-protein isoform Gq and PLCβ in HEK293 cells (45), other groups have reported that vascular endothelial cells also express $P2X_4$ receptor. This might contribute to the observed response, along with the metabotropic $P2Y_1$ and $P2Y_{11}$ receptors which are abundantly expressed in endothelial cells, thus largely contributing to vasodilation (70).

Our co-immunoprecipitation and FRET assays also revealed that the TRPC5-eNOS association is accelerated by intracellular Ca^{2+} elevation presumably through the formation of Ca^{2+}–CaM complex upon receptor stimulation (Fig. 5, A and B). Consistently, our TIRF imaging showed that eNOS-GFP accumulated at the plasma membrane after $[Ca^{2+}]_i$ elevation in HEK293 cells cotransfected with TRPC5 and eNOS-GFP, but dissipated in cells transfected with eNOS-GFP alone (Fig. 6B). This difference is at least in part attributable to redirection of eNOS from caveolin-1 to the C-terminus of TRPC5 (Fig. 5, G and H) and to enhanced levels of TRPC5 in the plasma membrane (63) (Fig. 6, A–C) upon $[Ca^{2+}]_i$ elevation. These results point to the importance of dynamic nature of the assembly comprised of TRPC5, eNOS, caveolin-1, and CaM in the vascular Ca^{2+}-NO signal coordination.

Our characterization of the TRPC5 and eNOS interaction through the mutagenesis of the TRPC5 caveolin-1–binding domain (residues 295–322) or eNOS caveolin-1–binding domain supports the hypothesis that TRPC5 and eNOS form a protein complex on caveolin-1. When this assembly is defective, the proximity effect that enables efficient transfer of NO from eNOS to TRPC5 *via* S-nitrosylation becomes insufficient, compromising Ca^{2+} signaling and NO release. We have previously reported that ATP-activated TRPC5-mediated Ca^{2+} entry is affected by blocking S-nitrosylation by mutating the relevant residue in TRPC5 (46). In addition, we have also reported that TRPC5 is resistant to ODQ, indicating that the downstream pathway of NO signal that produces cGMP is unlikely to be involved, supporting the importance of S-nitrosylation in TRPC5-mediated Ca^{2+} signaling. We can therefore say from the perspective of caveolin-1 targeting and NO-Ca^{2+} signal coordination that our finding adds a new mechanistic insight to the previously documented role of caveolin-1 governing the localization of TRPC1 and TRPC4 using caveolin-1 KO mice (22) or TRPV4 by pharmacological method (71) in endothelial cells.

TRPC5 has been shown to form functional heterotetramers with its closest homolog TRPC1 or TRPC4 in physiological conditions (65, 66, 72). In fact, a recent study reported that TRPC1/C4/C5-containing channels are mostly heteromers in rodent brain, but it could also form homomers (73). Although TRPC5 multimerization is not addressed in BAEC, it is assumed that the situation is similar to other cell types. Importantly, TRPC1- or TRPC4-expressing cells showed Ca^{2+} responses to NO after but not before TRPC5 co-expression (46), suggesting a key role of TRPC5 in determining the NO sensitivity and plasma membrane location of heteromeric channels.

A recent study reported the molar ratio of caveolin-1: eNOS in endothelial cells to be around 200:1 (74), caveolin-1 to be in far excess. Because the expression level of caveolin-1 is relatively low in HEK293 cells, we tested the effect of enhanced expression of caveolin-1. The overexpression of caveolin-1 mimicking the environment of endothelial cells showed the tendency to suppress (52%) the NO production, in agreement with the previous reports (75, 76), and Ca^{2+} influx as well (Fig. S2, C and D). However, the qualitative tendency of TRPC5 behavior *per se* was largely unaffected by caveolin-1 in terms of Ca^{2+} influx (Fig. S2C) and complex formation with eNOS (Figs. 5D and S5C), suggesting that the stoichiometry between caveolin-1 and eNOS or TRPC5 might not be stringently controlled. The overexpression of caveolin-1 nevertheless decelerated the kinetics of Ca^{2+} influx activation and TRPC5-eNOS association during ATP receptor stimulation (Figs. 5D, S2C, and S5C). This may be attributable to the synergetic effect of caveolin-1 multimerization that efficiently traps eNOS to prevent its dissociation from caveolin-1. Thus, for steering the ensemble between Ca^{2+} signal and NO production, the TRPC5–caveolin-1–eNOS

during 510 to 600 s (n = 7–8). p values are determined by one-way ANOVA with subsequent paired comparison. C, co-immunoprecipitation of eNOS-GFP with TRPC5-Flag under treatment with 100 μM ATP for the indicated time (min) in 0.5 mM EGTA- or 2 mM Ca^{2+}-containing solution. IPs with Flag-specific antibody are subjected to WB with antibody to GFP. D, time courses of the amount of bound proteins, normalized with respect to cell lysate protein concentrations (n = 3–7). p values are determined by two-way ANOVA with subsequent paired comparison. E, co-immunoprecipitation of eNOS-GFP with TRPC5-Flag under treatment with 100 μM ATP for the indicated time (min) in 2 mM Ca^{2+}-containing solution, using cell lysates obtained from HEK293 cells cotransfected with eNOS-GFP, CaM-Mut, and either TRPC5-Flag or Flag (left). Right, quantification of gel image. p values are determined by one-way ANOVA with subsequent paired comparison. F, $[Ca^{2+}]_i$ increases evoked by 100 μM ATP in 0.5 mM EGTA- or 2 mM Ca^{2+}-containing solution, in TRPC5-expressing HEK293 cells cotransfected with CaM constructs and either eNOS or vector. Averaged time courses (left) and maximal $[Ca^{2+}]_i$ increases in Ca^{2+}-containing solution (right) (n = 35–80). p values are determined by one-way ANOVA with subsequent paired comparison. G and H, pull down assay of eNOS with GST fusion proteins of TRPC5 fragments. GST fusion proteins immobilized on glutathione-Sepharose beads are incubated with cell lysates obtained from HEK293 cells cotransfected with eNOS-GFP and CaM in 100 nM (G) or 10 μM (H) Ca^{2+}-containing solution. Bound proteins are analyzed by WB with antibody to GFP (left). Right, quantification of gel image. p values are determined by one-way ANOVA with subsequent paired comparison. I, schematic illustration of TRPC5–caveolin-1–eNOS complex remodeling upon intracellular Ca^{2+} elevation. For B and F, individual data points indicate individual cells examined, and for all the gel images, individual data points indicate technical replicates. Data points are mean ± SD.
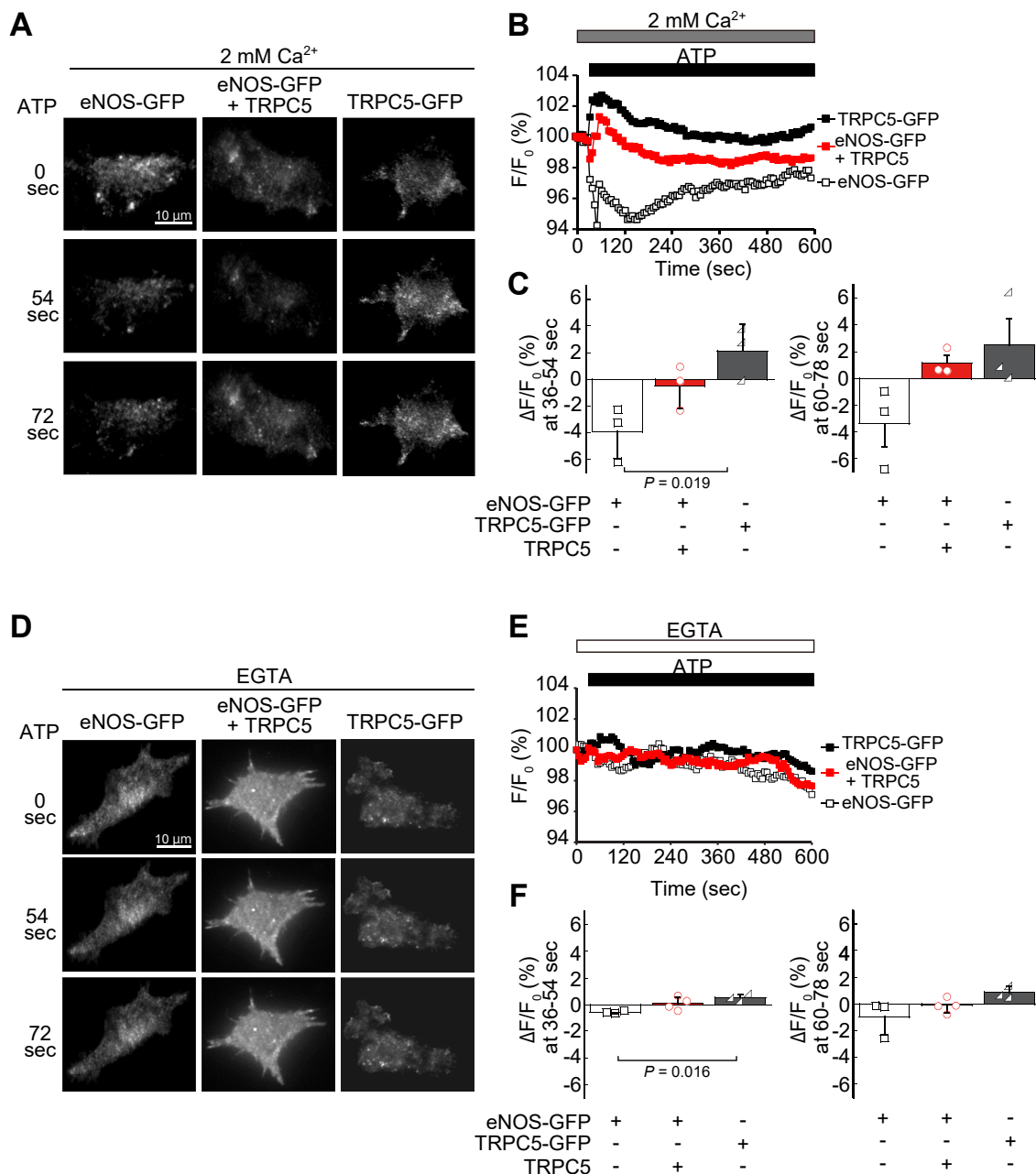
Figure 6. Plasma membrane dynamics of TRPC5 and eNOS during receptor stimulation. *A*, representative TIRF images from HEK293 cells expressing eNOS-GFP alone, eNOS-GFP plus TRPC5, or TRPC5-GFP alone upon treatment with 100 μM ATP in 2 mM Ca^{2+}-containing solution. *B*, averaged time courses of surface fluorescence changes (F/F_0) obtained by TIRF images from HEK293 cells in each condition upon treatment with 100 μM ATP in 2 mM Ca^{2+}-containing solution ($n = 3$). *C*, maximal surface fluorescence changes ($\Delta F/F_0$) at 36 to 54 s or 60 to 78 s ($n = 3$). *p* values are determined by one-way ANOVA with subsequent paired comparison. *D*, representative TIRF images from HEK293 cells expressing eNOS-GFP alone, eNOS-GFP plus TRPC5, or TRPC5-GFP alone upon treatment with 100 μM ATP in 0.5 mM EGTA-containing solution. *E*, averaged time courses of surface fluorescence changes obtained by TIRF images from HEK293 cells in each condition upon treatment with 100 μM ATP in 0.5 mM EGTA-containing solution ($n = 3$–4). *F*, maximal surface fluorescence changes at 36 to 54 s or 60 to 78 s in 0.5 mM EGTA-containing solution ($n = 3$–4). *p* values are determined by one-way ANOVA with subsequent paired comparison. Data points are mean ± SD. For *C* and *F*, individual data points indicate individual cells examined.

tertiary complex possesses the caveolin-1–mediated negative regulatory mechanism, which is neutralized by Ca^{2+}-CaM, in addition to the positive regulatory mechanism *via* the proximity effect and *S*-nitrosylation.

The results of our confocal microscopy analysis also agree with several other reports which claim that the existence of caveolin-1 does not affect the localization of eNOS using KO mice (53, 54). This may be due to possible

unknown binding of the N-terminus of caveolin-1, although the well-known putative protein-binding motif located on the C-terminus side is deleted in the KO mice. Interestingly, in this context, while the TRPC5 CBD mutant TRPC5$_{Y296A/F301A}$ lacks the ability to bind caveolin-1 that mediates the complex formation with eNOS, both TRPC5$_{Y296A/F301A}$ and eNOS are present in the plasma membrane (Fig. 4*C*), suggesting that TRPC5 and eNOS
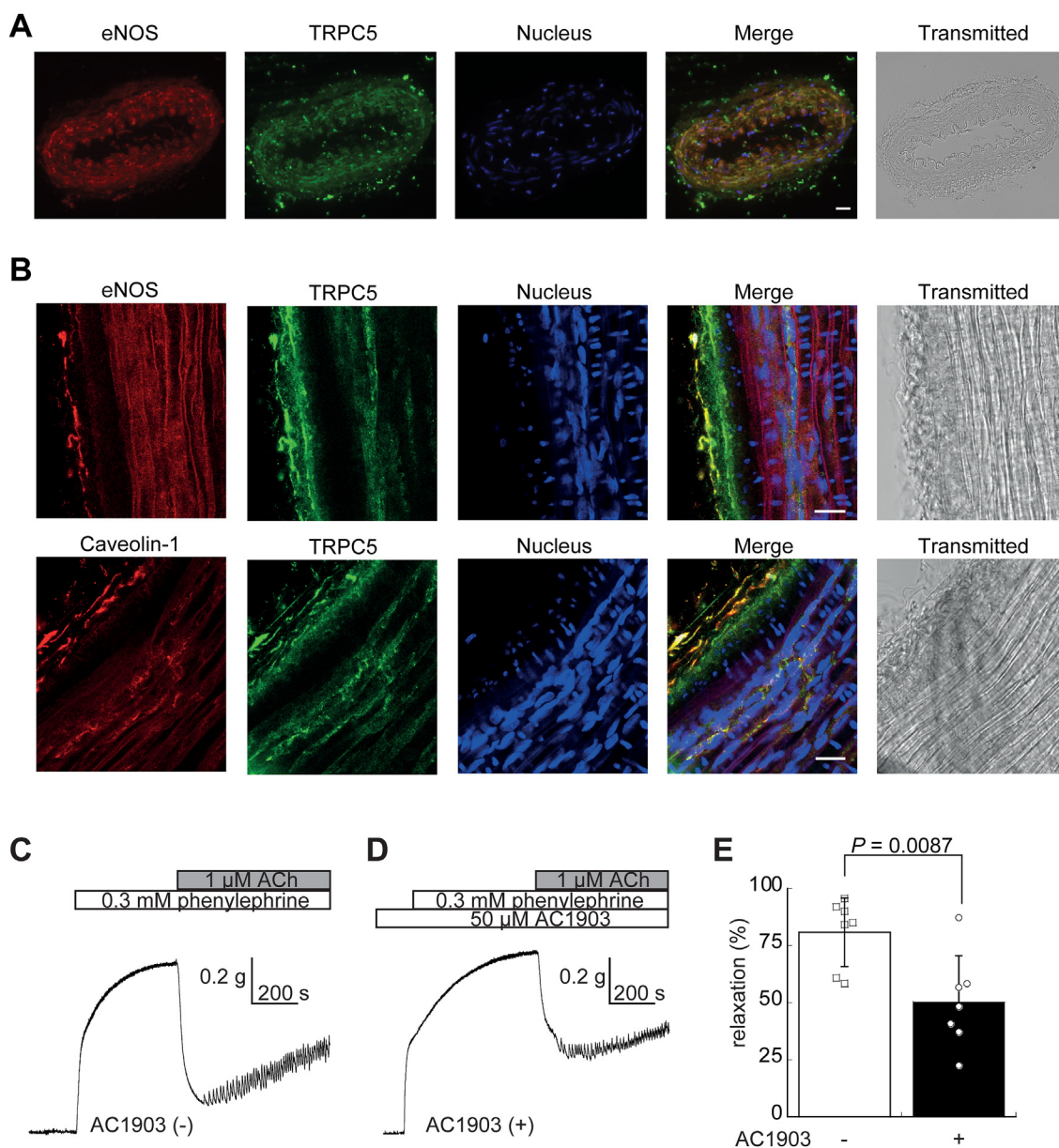
Figure 7. Selective TRPC5 inhibition suppresses acetylcholine-induced relaxation of rat aorta. *A*, localization of TRPC5 and eNOS in the endothelium of mesenteric arteries isolated from rat *in situ* under whole-mount staining visualized by confocal microscopy shown *en face*. The bar indicates 20 μm. *B*, localization of TRPC5 and eNOS, and caveolin-1 in the endothelium of mesenteric arteries isolated from rat *in situ* under whole-mount staining visualized by confocal microscopy. Anti-TRPC5 antibody (*green*), anti-eNOS antibody (*red*), and anti-caveolin-1 antibody (*red*) are used. The nuclei are stained with Hoechst 33342 (*blue*). The bar indicates 20 μm. *C*, representative time course of acetylcholine-induced relaxation of isolated rat aorta. *D*, representative time course of acetylcholine-induced relaxation of isolated rat aorta pretreated with 50 μM AC1903. In *C* and *D*, 0.3 mM phenylephrine is first added to the bath solutions to induce maximum contraction. *E*, averaged relaxation of rat aorta (n = 7). Individual data points indicate biological replicates. Data points are mean ± SD.

alone or in combination possess an intrinsic ability to translocate to the plasma membrane.

Caveolin-1 is known to interact with many signal transduction proteins including vasodilator receptors, G-proteins, PLCs, kinases, and phosphatases in endothelial cells (17, 20). Although it is still unclear how multiple signal transduction proteins interact simultaneously with caveolin-1, accumulated evidence has suggested that oligomerization of caveolin-1 at the plasma membrane allows it to bind multiple proteins (77). Indeed, TRPC1, which assembles into hetero-tetrameric channels with TRPC5 (46, 78), forms indirect protein complexes with IP_3 receptors *via* caveolin-1 (79). Therefore, additional signaling proteins, such as vasodilator receptors, other TRP channels, PLC, Akt, PKA, and PKC, which are functionally linked to the activation of TRPC5 and eNOS, can be assembled with TRPC5 and eNOS through caveolin-1 oligomers to regulate Ca^{2+} and NO signaling in endothelial cells. Interestingly, a previous report has shown that, following Ca^{2+} store depletion, caveolin-1 targets and retains TRPC1 within the ER-plasma junctional membrane regions to assist
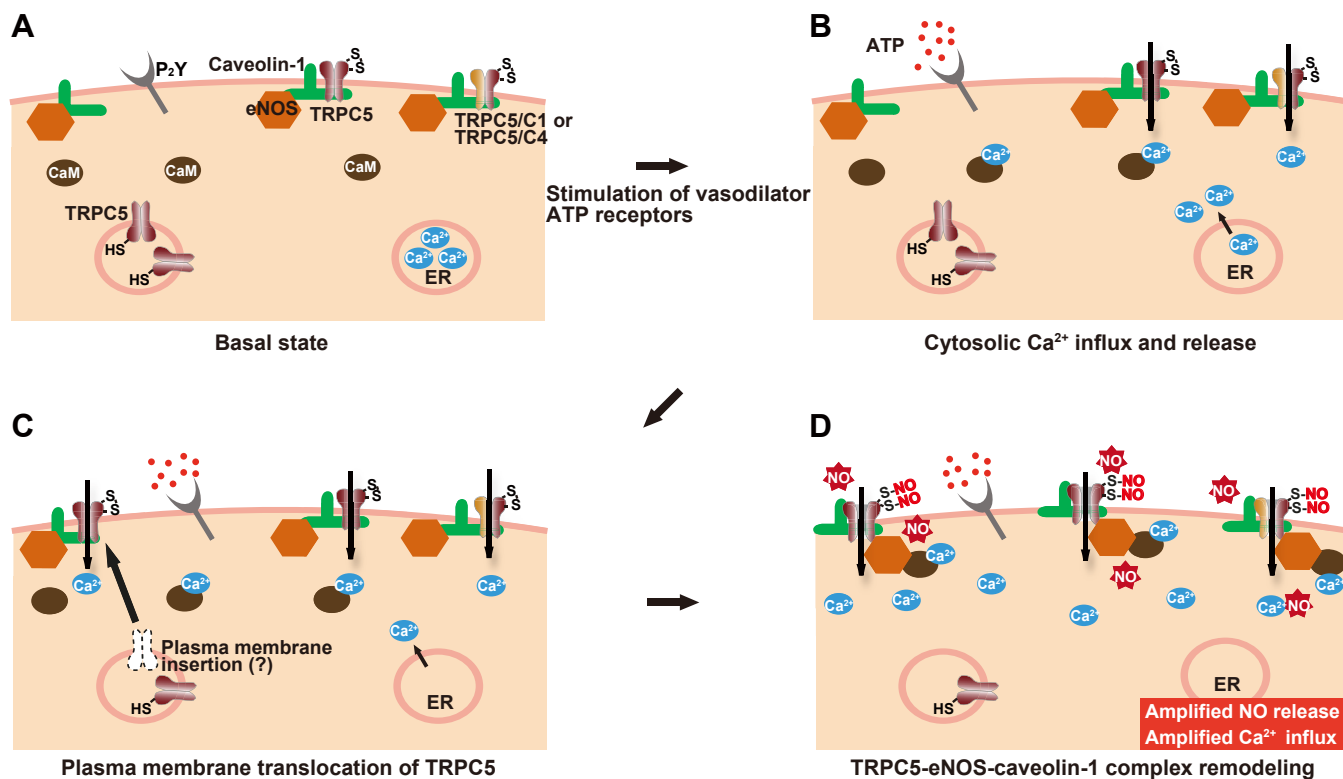
Figure 8. A proposed model for dynamic interaction among TRPC5 channel, caveolin-1, and eNOS coordinating interplay between Ca²⁺ and NO signals. *A*, in the resting state, caveolin-1 provides a scaffold for the assembly of TRPC5 and eNOS into a protein complex. *B*, upon stimulation of vasodilator receptors, Ca²⁺ influx *via* TRPC5 is induced through the PLC cascade to evoke the primary rise of $[Ca^{2+}]_i$, activating CaM. *C*, primary increase of $[Ca^{2+}]_i$ triggers the plasma membrane translocation of TRPC5 and thus increases the number of TRPC5–caveolin-1–eNOS assembly. *D*, the assembly is likely to increase the efficiency of the association of eNOS with Ca²⁺-CaM, which releases eNOS from caveolin-1 and allows eNOS to interact with the C-terminus of TRPC5 (residues 936–975). This proposed model enables eNOS to produce NO in the vicinity of TRPC5, optimizing secondary activation of TRPC5 through *S*-nitrosylation and consequently amplifying Ca²⁺ signaling.

its association with STIM1, which does not itself associate with caveolin-1 (19). Mutation of the caveolin-1–binding domain in TRPC1 dramatically decreases the association between TRPC1 and STIM1 without affecting STIM1 localization and thereby reduces the store-operated channel activity of TRPC1. Further study is still necessary to clarify the importance of other caveolin-1–associated proteins in the TRPC5–eNOS complex.

NO is highly reactive and diffusible within cells, posing the question of how *S*-nitrosylation–dependent regulation of cellular signaling is achieved with any selectivity. Our present study suggests that it is achieved by maximizing the subcellular proximity of eNOS and TRPC5 (Figs. 1*E* and 8*D*). Another good example of this proximity effect is the NMDAR–nNOS complex, in which PSD-95 acts as a scaffolding protein and mediates protein–protein interactions that couple NMDAR with nNOS (15, 80). This protein complex enables nNOS to produce NO in the vicinity of NMDARs, leading to an efficient inhibition of the Ca²⁺ channel activity of NMDAR through *S*-nitrosylation. In addition to the proximity effect, recent studies have demonstrated that selectivity is conferred upon *S*-nitrosylation signaling pathways through transnitrosylation, a transfer of the NO group between interacting proteins in the absence of apparent NO release (81). Importantly, our recent study demonstrated that transnitrosylating *N*-nitrosamine compounds selectively activate TRPA1 channels (24). Thus,

analogously for the TRPC5 channel and NMDAR, NO signaling specificity can be achieved through subcellular proximity effects and by transnitrosylation. These mechanisms may provide the molecular basis for the direct regulation of TRP channels by NO, which has been the issue among different groups (24, 46, 48–50).

Our immunolocalization studies have revealed that TRPC5 is distributed on both the luminal and abluminal membrane in the endothelial cell layer in vascular tissue. Given that vasodilator receptors are distributed at the luminal surface of the endothelial cell layer (82), NO initially produced there may diffuse throughout the cytoplasm to activate TRPC5 in the abluminal membrane, thus propagating Ca²⁺ signals from the luminal membrane toward the abluminal membrane. This mechanism may contribute to global $[Ca^{2+}]_i$ rises and full activation of eNOS in the Golgi (83) of endothelial cells, eventually leading to synchronization of neighboring smooth muscle cells during vascular relaxation at the whole-tissue level. This idea is substantiated by the fact that genetic disruption of TRPC4, the closest TRPC5 relative colocalized with TRPC5 in the endothelial cell membrane (46), impairs agonist-dependent vasorelaxation (84). The TRPC5 channel–caveolin-1–eNOS signaling complex could also be involved in the activation of eNOS by shear stress (27) because membrane stretch has been reported to activate TRPC5 independently of

the PLC cascade (85). While shear stress-activated NO production can be initiated independently of Ca^{2+} (27), the secondary amplification phase of this mode of NO production may be mediated by Ca^{2+} influx *via* NO-activated TRPC5 channels. Thus, the positive feedback regulation of Ca^{2+} and NO signals by NO-activated TRPC5 channels is likely to play important roles in robustifying the responses of endothelial cells.

Experimental procedures

Cell culture and cDNA expression

BAEC and HEK293 were obtained from ATCC. BAECs were cultured in phenol red–free Dulbecco's modified Eagle's medium (DMEM) (Gibco) containing 10% fetal bovine serum (FBS), 30 U ml^{-1} penicillin, 1 μM all-trans-retinoic acid, and 30 μg ml^{-1} streptomycin at 37 °C/5% CO_2, as previously reported (46). To remove retinoid hormones, FBS was incubated with 0.5% dextran-coated charcoal (Sigma) at 4 °C overnight. BAECs were used between passages 3 to 7. Transfection was carried out using Lipofectamine 2000 (Invitrogen). HEK293 cells were cultured in DMEM containing 10% FBS, 30 U ml^{-1} penicillin, and 30 μg ml^{-1} streptomycin. For the $[Ca^{2+}]_i$ imaging and electrophysiological measurements, HEK293 cells were cotransfected with recombinant plasmids and pEGFP-F (Clontech) as a transfection marker, using SuperFect Transfection Reagent (QIAGEN). BAECs and HEK293 cells were trypsinized, diluted with DMEM, and plated onto glass coverslips 24 h after transfection. The cells were subjected to measurements 8 to 24 h after plating.

siRNA experiments

The sense siRNA sequences 5′-AATGCCTTCTC-CACGCTCTTT-3′ for bovine TRPC5 and 5′-AATATCCTG-GAGGATGTGGCC-3′ for bovine eNOS were used (46). The randomized siRNA target sequences were 5′-AATCGCCTCTTACGCTCCTTT-3′ and 5′-AATGCGTGT TGCTAGACGCAG-3′, respectively. Computer analysis confirmed this sequence to be a specific target that has no homology to other bovine genes. The Silencer siRNA Construction Kit (Ambion) was used to construct the siRNA oligomers, which were then transfected into BAECs using Lipofectamine 2000 (Invitrogen). siRNA for caveolin-1 was purchased from Santa Cruz.

Efficiency of siRNA in BAEC was validated by quantitative reverse transcription-PCR (RT-PCR) using the following primer sets: TRPC5 FW: 5′- TGATCGCCATGATGAACAAC -3′, TRPC5 RV: 5′- TTGTTGAACCAGTTGCCAAG -3′; eNOS FW: 5′- AGGAGTGGAAGTGGTTCCG -3′ and eNOS RV: 5′- TGACAGAGTAGTACCGGGGC -3′; caveolin-1 FW: 5′- GCATCAACACGCAGAAAGAA -3′, caveolin-1 RV: 5′- AGACAACCCCCAACACAGAC -3′; 18S rRNA: FW: 5′- GGTAGTGACGAA AAATAACAATACAGGA -3′, RV: 5′- ATACGCTATTGGAGCTGGAATTACC -3′. Samples were prepared using One Step TB Green PrimeScript RT-PCR Kit (Takara) by following the manufacturer's protocol. Quantitative RT-PCR was performed using QuantStudio (Thermo Fisher Scientific). Gene amplification was quantified by $\Delta\Delta Ct$ method using 18S rRNA as endogenous control.

$[Ca^{2+}]_i$ imaging

Cells on coverslips were loaded with 1 μM fura-2 AM (Dojindo) in DMEM containing 10% FBS at 37 °C for 40 min. The coverslips were then plated in a perfusion chamber mounted on the stage of the microscope. Fluorescence images of the cells were recorded and analyzed with a video image analysis system (AQUACOSMOS; Hamamatsu Photonics). Fura-2 fluorescence at an emission wavelength of 510 nm was obtained at room temperature (21 °C) by exciting fura-2 alternately at 340 and 380 nm. The 340:380 ratio was obtained on a pixel-by-pixel basis. Reagents dissolved in water or dimethyl sulfoxide were diluted to their final concentrations in HBS (containing (in mM): 107 NaCl, 6 KCl, 1.2 $MgSO_4$, 2 $CaCl_2$, 11.5 glucose, 20 Hepes; adjusted to pH 7.4 with NaOH) or Ca^{2+}-free HBS (containing (in mM): 107 NaCl, 6 KCl, 1.2 $MgSO_4$, 0.5 EGTA, 11.5 glucose, 20 Hepes; adjusted to pH 7.4 with NaOH) and applied to the cells by perfusion. Since NOS fails to produce NO in the absence of a sufficient concentration of L-arginine, 3 mM L-arginine was added to solutions used for BAECs and HEK293 cells transfected with eNOS constructs.

Intracellular NO imaging

NO production was measured by the esterase-sensitive NO-sensitive fluorescent dye, DAF-2 DA (Daiichi Pure Chemicals). Cells were loaded with 10 μM DAF-2 DA for 15 min at 37 °C. DAF-2 fluorescence was measured using the same equipment as for the $[Ca^{2+}]_i$ imaging but with a different filter set (excitation at 490 nm, emission at 515 nm). To decrease quenching of DAF-2 fluorescence, excitation was performed at 30 s intervals. Three millimolars of L-arginine was added to the bath solutions. Data are presented as the ratio of the fluorescence intensity at each point divided by the fluorescence intensity at the start of the experiment (F/F_0).

S-nitrosylation assays

The *S*-nitrosylation assay (biotin switch assay) was performed as previously described (46). Briefly, BAECs were incubated with ATP (1 μM) in the dark at room temperature for 5 to 30 min, and HEK293 cells expressing TRPC5-GFP and eNOS constructs were incubated with ATP (100 μM) at room temperature for 10 min. The cells were washed with PBS, harvested, and lysed in RIPA buffer (pH 8.0) containing 150 mM NaCl, 1% Nonidet P-40, 0.5% sodium deoxycholate, 0.1% SDS, and 50 mM Tris. The extracts were incubated with 100 mM methylmethanethiosulfonate and 2.5% SDS at 50 °C for 30 min before the methylmethanethiosulfonate was removed by precipitation with an equal volume of cold (−30 °C) acetone. After resuspending the proteins in HEN buffer (250 mM Hepes pH 7.7, 1 mM EDTA, and 0.1 mM neocuproine) containing 1% SDS, we added sodium ascorbate (1 mM final concentration) and *N*-[6-(biotinamido)hexyl]-3′-(2′-pyridyldithio)propionamide (biotin-HPDP) (1 mM final

concentration, Thermo Fisher Scientific). The mixtures were incubated for 1 h at 25 °C in the dark with intermittent vortexing. Biotinylated nitrosothiols were then acetone-precipitated with two volumes of cold (−30 °C) acetone to remove residual biotin-HPDP. After centrifugation, the pellet was resuspended in 0.1 ml HEN buffer containing 1% SDS. Two volumes of neutralization buffer (20 mM Hepes (pH 7.7), 100 mM NaCl, 1 mM EDTA, and 0.5% Triton X-100) were added, and biotinylated proteins were incubated with NeutrAvidin-Plus beads for 1 h at room temperature. The resin was extensively washed in 10 volumes of neutralization buffer containing 600 mM NaCl. The proteins were eluted in sample buffer containing 50 mM DTT at room temperature for 30 min and analyzed by 7.5% SDS PAGE and western blotting using antibodies against TRPC5 (Alomone Labs) or GFP (Clontech). The intensity of the signals was quantified by Image J software and normalized by the input signal.

Co-immunoprecipitation of endogenous TRPC5 with eNOS and caveolin-1

BAECs were lysed in RIPA buffer and the cell extract was immunoprecipitated with an antibody against eNOS (CALBIOCHEM) or caveolin-1 (Santa Cruz Biotech) in the presence of protein-A-sepharose beads (GE Healthcare) with rocking for 4 h at 4 °C. The immune complexes were washed three times with RIPA buffer and resuspended in SDS sample buffer containing 50 mM DTT for 2 h at room temperature. The proteins were analyzed by 7.5% SDS-PAGE and western blotting using an antibody against TRPC5 (Alomone Labs). The intensity of the signals was quantified by Image J software and normalized by the lysate signal.

Confocal immunovisualization

BAECs treated with retinoic acid (1 μM) for 4 days were seeded in a glass-bottomed culture dish and were fixed with 3% (v/v) paraformaldehyde in PBS for 15 min at room temperature, washed with PBS, and then permeabilized with 0.2% (v/v) Triton X-100 in PBS for 10 min at room temperature. After washing three times with PBS, the cells were incubated with 5% bovine serum albumin in PBS for 1 h at room temperature. The cells were then incubated for 1 h at room temperature with anti-TRPC5 goat polyclonal antibody (Santa Cruz Biotech C17) and anti-eNOS mouse monoclonal antibody (CALBIOCHEM) or anti-caveolin-1 rabbit polyclonal antibody (Santa Cruz Biotech), each diluted in Can Get Signal immunostain (TOYOBO). After washing with PBS three times, samples were incubated with Hoechst 33342 (Dojindo) together with DyLight 488 anti-goat IgG to detect TRPC5, DyLight 549 anti-mouse IgG to detect eNOS, or DyLight 549 anti-rabbit IgG to detect caveolin-1 at room temperature for 1 h. After washing three times with PBS, the dishes were stored at 4 °C before imaging. Fluorescence images were acquired with a confocal laser-scanning microscope (TCS SP8, Leica). Hoechst 33342 was excited by a diode 405 nm laser and fluorescence detected by photo-multipliers in the range of 410 to 480 nm. DyLight 488 and DyLight 549 were excited by diode 488 and 552 nm lasers,

respectively. Fluorescence was detected by HyD detectors in the range of 500 to 558 nm for DyLight 488 and 560 to 650 nm for DyLight 549. The specimens were viewed at high magnification using HC PL APO CS2 oil objectives (63×, 1.40 NA, Leica). For proximity ligation assay, Duolink PLA starter kit (Sigma-Aldrich) was used according to the manufacturer's instructions. Briefly, HEK293 cells expressing TRPC5 and eNOS constructs or BAECs were cultured on a glass-bottom dish (Mattek). The cells were fixed by 4% PFA, followed by blocking for 1 h at 37 °C using the provided blocking buffer. The cells were then incubated for 1 h at room temperature with anti-TRPC5 goat polyclonal antibody (Santa Cruz Biotech C17, 1:1000) and anti-eNOS mouse monoclonal antibody (CALBIOCHEM, 1:1000), followed by incubation with Duolink PLA Probes for 1 h at 37 °C. The samples were then incubated with the provided ligation mix for 30 min at 37 °C, followed by amplification for 100 min at 37 °C by DNA polymerization. Samples were mounted with Duolink In Situ Mounting Media with DAPI and the fluorescence signals were observed by LSM 780 (Carl Zeiss). For quantification of the colocalization of TRPC5 and eNOS, the images were split to respective channels and the number of pixels containing both eNOS and TRPC5 signals were divided by the number of pixels showing TRPC5 signals alone to obtain the relative area of colocalization.

Whole-mount immunostaining

Rat mesenteric artery was cleaned of fat and connective tissue, and luminal blood was removed. After brief fixation in 3.4% paraformaldehyde in PBS for 1 h at room temperature, segments were incubated in 0.1% Triton X-100 and 2% bovine serum albumin dissolved in PBS for 1 h at 37 °C. Primary antibodies (anti-TRPC5 polyclonal antibody (Santa Cruz Biotech) and anti-eNOS monoclonal antibody (Calbiochem) or anti-caveolin-1 polyclonal antibody (Santa Cruz Biotech)) were diluted in Can Get Signal immunostain (TOYOBO) and applied to the fixed vessels over night at 4 °C. Following a PBS rinse, samples were incubated with Hoechst 33342 (Dojindo) together with Alexa Fluor 647-conjugated anti-goat IgG to detect TRPC5 and DyLight 549-conjugated anti-mouse IgG to detect eNOS or DyLight 549-conjugated anti-rabbit IgG to detect caveolin-1 diluted in Can Get Signal immunostain for 1 h at 37 °C, then rinsed three times with PBS and permanently mounted. The preparations were then visually examined using a TCS SP8 confocal microscope system using a Leica HC PL APO CS2 40× oil immersion objective (NA = 1.30). Hoechst 33342 was excited by a diode 405 nm laser and emitted fluorescence was detected by photo-multiplier in the range of 410 to 480 nm. DyLight 549 and Alexa Fluor 647 were excited by diode 552 and 638 nm lasers, respectively. Fluorescence was detected by HyD detectors in the range of 558 to 625 nm for DyLight 549 and 650 to 710 nm for Alexa Fluor 647, and photographs were taken with the focus on the intima as judged by the pattern of nuclear staining. Images were digitized under constant sampling rate, gain and offset.

Plasmid construction for expression in mammalian cells

Mouse TRPC5 and human eNOS were tagged at the C-terminus with Flag, GFP, Ds-Red, CYP, or YFP as described previously (46, 86). TRPC5$_{Y6A/Y11A/Y14A}$ and TRPC5$_{Y296A/F301A}$ were constructed using the QuikChange Site-Directed Mutagenesis Kit (Stratagene). The primer pairs used for TRPC5$_{Y6A/Y11A/Y14A}$ and TRPC5$_{Y296A/F301A}$ were as follows: 5′-CTGTACGCCAAGAAGGTCAATGCCTCACCA-TAC-3′ and 5′-GTATGGTGAGGCATTGACCTTCTTGGC GTACAG-3′ for Y6A/Y11A; 5′-CCTCACCAGCCAGA-GATCGCATCCCCCTCC-3′ and 5′-GGAGGGGGATGC-GATCTCTGGCTGGTGAGG-3′ for Y14A; 5′-ATCAA AGCTCACCAGAAAGAGGCTGTCGTTC-3′ and 5′-GAAC-GACAGCCTCTTTCTGGTGAGCTTTGAT-3′ for Y296A/F301A. For production of GST fusion proteins of the TRPC5 fragments (residues 1–330, 352–398, 625–975, 625–935, and 625–954), the genes encoding the TRPC5 fragments and the GST were subcloned together into the *Eco*RI and *Sal*I sites of the pET23 vector (Novagen).

Co-immunoprecipitation in HEK293 cells

At 48 h after transfection, HEK293 cells were lysed in RIPA buffer. The cell lysate was immunoprecipitated with M2 monoclonal antibody to Flag (Sigma) in the presence of Protein A Sepharose beads (GE Healthcare) with rocking for 4 h at 4 °C. The immune complexes were washed three times with RIPA buffer and resuspended in SDS sample buffer containing 50 mM DTT for 30 min at room temperature. The proteins were analyzed by 7.5% SDS-PAGE and western blotting using an anti-GFP antibody (Clontech). The intensity of the signals was quantified by Image J software and normalized by the lysate signal.

Electrophysiological measurements

Whole-cell currents were recorded at room temperature using the conventional whole-cell patch clamp technique with an EPC9 amplifier (Heka) as described previously (87). The patch electrodes were prepared from borosilicate glass capillaries and had a resistance of 2 to 4 MΩ. Series resistance was compensated (to 70–80%) to minimize voltage errors. Current signals were filtered at 5 kHz with a four-pole Bessel filter and digitized at 10 kHz. The PatchMaster (Heka Electronics) software was used for command pulse control, as well as data acquisition and analysis. The cells were maintained at −50 mV, and the currents were measured by voltage ramps (from −100 mV to +100 mV; 50 msec duration). The standard pipette-filling solution contained the following: CsOH, 117.7 mM; L-aspartate, 103 mM; CsCl, 40 mM; CaCl$_2$, 1.31 mM; MgCl$_2$, 2 mM; EGTA, 5 mM; Hepes, 5 mM; Na$_2$ATP, 2 mM; NaGTP, 0.1 mM; adjusted to pH 7.25 with CsOH (50 nM calculated free Ca^{2+}). The osmolarity of the pipette-filling solution was adjusted to ≈291 mOsm. The "2 mM Ca^{2+}" external solution contained the following: NaCl, 125 mM; MgCl$_2$, 1.2 mM; CaCl$_2$, 2 mM; glucose, 10 mM; Hepes, 11.5 mM; mannitol, 29 mM; L-arginine, 3 mM; adjusted to pH 7.4 with NaOH. The "EGTA" external solution

contained the following: NaCl, 121.7 mM; MgCl$_2$, 1.2 mM; CaCl$_2$, 1.2 mM; EGTA, 2 mM; glucose, 10 mM; Hepes, 11.5 mM; mannitol, 30 mM; L-arginine, 3 mM; adjusted to pH 7.4 with NaOH. The osmolarity of the external solutions was adjusted to ≈295 mOsm.

GST pull-down binding assay

All GST fusion proteins were expressed in the Rosetta strain of *Escherichia coli* (Novagen) and affinity-purified using glutathione-Sepharose 4B beads (GE Healthcare). Other proteins used for the binding assays were obtained from HEK293 cells transfected with caveolin-1-GFP, eNOS-GFP, or CaM. At 48 h after transfection, the cells were lysed in RIPA buffer and the extracts were centrifuged at 17,400g for 20 min. The supernatant was incubated with glutathione-Sepharose beads bound with GST-fused TRPC5 fragments for 2 h in RIPA buffer containing 0.1 or 10 μM CaCl$_2$. The beads were then washed, and the proteins retained on the beads were characterized by 7.5% SDS-PAGE and western blotting using anti-GFP or anti-GST antibodies (Clontech). The intensity of the signals was quantified by Image J software.

FRET imaging

HEK293 cells expressing TRPC5-CFP and YFP, or TRPC5-CFP and eNOS-YFP, were rinsed once with HBS solution containing 2 mM Ca^{2+} and imaged in the same solution. Images were acquired on an inverted microscope equipped with an autofocus system (IX81-ZDC2; Olympus) using a high-sensitivity EM-CCD camera (ImagEM; Hamamatsu Photonics) controlled by MetaFluor software (Molecular Devices). CFP and FRET images were obtained every 5 s through a 427/10 nm excitation filter and either a 472/30 nm emission filter (for CFP) or a 542/27 nm emission filter (for FRET). Images were analyzed using MetaFluor software. One region per cell was selected such that there was no net movement of the targeted reporter in and out of the selected region. To analyze the changes of FRET ratio in the area of the plasma membrane, regions of interest(ROI) were defined over the outer border (typical region thickness: 0.5 μm), and the average FRET/CFP ratio within the ROI was calculated using MetaFluor software. Baseline images were acquired for 1 min before adding 100 μM ATP. Data are presented as the FRET/CFP ratio normalized to that at t = 0.

TIRF microscopy

TIRF images were acquired using a TIRF illumination system (IX2-RFAEVA-2, Olympus) mounted on an inverted microscope equipped with an autofocus system (IX81-ZDC2; Olympus). A diode-pumped solid state 488-nm laser (kyma488, 10 mW; Melles Griot) was used for total fluorescence illumination, and a 510 nm long-pass filter was used as an emission filter. Images were captured with a high-sensitivity EM-CCD camera (ImagEM; Hamamatsu Photonics) operated with MetaMorph software (Molecular Devices). HEK293 cells expressing eNOS-GFP alone, eNOS-GFP and TRPC5, or TRPC5-GFP alone were plated onto poly-L-lysine–coated

glass coverslips (Iwaki) and placed in a custom chamber with HBS solution containing 2 mM Ca^{2+} or EGTA at room temperature. Prior to the addition of any agents, cells were first imaged for 1 min to establish the baseline. For fluorescence intensity analysis, ROI with areas between 5 to 10% of the visible footprint of individual cells were drawn. Data are presented as the ratio of the fluorescence intensity at each point divided by the fluorescence intensity at the start of the experiment (F/F_0), where each value was background-subtracted to correct for the dark-field noise of the camera. Images were captured every 5 s.

RNA isolation and RT-PCR

HEK293 cells were treated with 1 ml Isogen (Nippon Gene) and total RNA was obtained according to the manufacturer's protocol. Isolated total RNA was reverse-transcribed to cDNA using oligo-dT primers according to the manufacturer's protocol. PCR was performed using sense (5′-GACTTTGAA-GATGTGATTGCAGAAC-3′) and antisense (5′-GCAA GTTGATGCGGACATTGC-3′) primers for human caveolin-1 gene (GenBank: Z18951) and sense (5′-ATGTACAAGTT CCTGACGGTGTTC-3′) and antisense (5′-CAATCC TGGCTCAGTTGCAGG-3′) primers for human caveolin-2 gene (GeneID:NG_029920), respectively. PCR conditions were 94 °C for 30 s, 42 °C for 30 s, and 70 °C for 30 s, for 30 cycles. The RT-PCR products were resolved under agarose gel electrophoresis and cDNA amplicons corresponding to the predicted product sizes were purified using the QIAquick Gel Extraction kit (Qiagen Inc). The resultant cDNA fragments were ligated into pGem-T Easy vector (Promega Corp) and transformed into DH5α competent cells. Positive clones were selected and sequenced using T7 promoter primers by ABI prism DNA sequencer (GeneMed Synthesis Inc).

Measurement of endothelium-derived NO-dependent relaxation in rat aorta

Animal experiments were approved by the Experimental Animal Committee of Teikyo Heisei University (Dou2023-1). Male Wistar rats, 7 to 8 weeks old (250–280 g; CLEA Japan, Inc.), were killed by decapitation under anesthesia with 3% isoflurane. The thoracic aortae were dissected from the rats and were cleaned of fat and adhering connective tissue. Blood clots in the lumen were flushed out with ice-cold oxygenated (95% O_2-5% CO_2) physiological saline solution of the following composition (mmol/L): NaCl 118, KCl 4.7, $CaCl_2$ 2.5, KH_2PO_4 1.18, $MgSO_4$ 1.18, $NaHCO_3$ 15, EDTA 0.026, and glucose 11. The aortae were cut transversely into 3-mm lengths rings, and the rings were cut into strips. The aortae were set up in a 5-ml organ bath with water-jacketed chambers for isometric force measurement. The solution was maintained at 37 °C and bubbled with 95% O_2-5% CO_2 (pH 7.4). The aortae were equilibrated for 40 min and were periodically stretched to obtain a resting tension of 1 g. After the equilibration period, the aortae were contracted with 80 mM KCl until successive challenges gave stable contractions of equivalent magnitudes. The aortae were used to measure the endothelium-derived NO-dependent relaxation.

Statistical analyses

Data are expressed as the mean ± SD, unless otherwise stated. We accumulated the data for each condition from at least three independent experiments. Statistical significance was determined with the unpaired, 2-tailed Student's *t* test for comparisons between two mean values and 1-way or 2-way ANOVA for comparisons between multiple data sets as stated in the figure legend, with a value of $p < 0.05$ considered to be significant. For ANOVA, Tukey's HSD was used for *post hoc* testing method.

Data availability

All data generated or analyzed during this study are included in this article or are available from the corresponding author (Yasuo Mori, E-mail: mori@sbchem.kyoto-u.ac.jp) upon reasonable request.

References

1. Clapham, D. E. (2003) TRP channels as cellular sensors. *Nature* **426**, 517–524
2. Voets, T., Talavera, K., Owsianik, G., and Nilius, B. (2005) Sensing with TRP channels. *Nat. Chem. Biol.* **1**, 85–92
3. Putney, J. W., and Tomita, T. (2012) Phospholipase C signaling and calcium influx. *Adv. Biol. Regul.* **52**, 152–164
4. Venkatachalam, K., and Montell, C. (2007) TRP channels. *Annu. Rev. Biochem.* **76**, 387–417
5. Hofmann, T., Obukhov, A. G., Schaefer, M., Harteneck, C., Gudermann, T., and Schultz, G. (1999) Direct activation of human TRPC6 and TRPC3 channels by diacylglycerol. *Nature* **397**, 259–263
6. Patterson, R. L., van Rossum, D. B., Ford, D. L., Hurt, K. J., Bae, S. S., Suh, P. G., *et al.* (2002) Phospholipase C-gamma is required for agonist-induced Ca^{2+} entry. *Cell* **111**, 529–541
7. Nishida, M., Sugimoto, K., Hara, Y., Mori, E., Morii, T., Kurosaki, T., *et al.* (2003) Amplification of receptor signalling by Ca^{2+} entry-mediated translocation and activation of PLCgamma2 in B lymphocytes. *EMBO J.* **22**, 4677–4688
8. Numaga, T., Nishida, M., Kiyonaka, S., Kato, K., Katano, M., Mori, E., *et al.* (2010) Ca^{2+} influx and protein scaffolding via TRPC3 sustain PKCbeta and ERK activation in B cells. *J. Cell Sci.* **123**, 927–938
9. Mori, Y., Kajimoto, T., Nakao, A., Takahashi, N., and Kiyonaka, S. (2011) Receptor signaling integration by TRP channelsomes. *Adv. Exp. Med. Biol.* **704**, 373–389
10. Tang, Y., Tang, J., Chen, Z., Trost, C., Flockerzi, V., Li, M., *et al.* (2000) Association of mammalian Trp4 and phospholipase C isozymes with a PDZ domain-containing protein, NHERF. *J. Biol. Chem.* **275**, 37559–37564
11. Storch, U., Forst, A. L., Pardatscher, F., Erdogmus, S., Philipp, M., Gregoritza, M., *et al.* (2017) Dynamic NHERF interaction with TRPC4/5 proteins is required for channel gating by diacylglycerol. *Proc. Natl. Acad. Sci. U. S. A.* **114**, E37–E46
12. Ong, H. L., and Ambudkar, I. S. (2011) The dynamic complexity of the TRPC1 channelosome. *Channels* **5**, 424–431
13. Polat, O. K., Uno, M., Maruyama, T., Tran, H. N., Imamura, K., Wong, C. F., *et al.* (2019) Contribution of coiled-coil assembly to Ca^{2+}/calmodulin-dependent inactivation of TRPC6 channel and its impacts on FSGS-associated phenotypes. *J. Am. Soc. Nephrol.* **30**, 1587–1603
14. Moncada, S., Palmer, R. M., and Higgs, E. A. (1991) Nitric oxide: physiology, pathophysiology, and pharmacology. *Pharmacol. Rev.* **43**, 109–142
15. Hess, D. T., Matsumoto, A., Kim, S. O., Marshall, H. E., and Stamler, J. S. (2005) Protein S-nitrosylation: purview and parameters. *Nat. Rev. Mol. Cell Biol.* **6**, 150–166
16. Rothberg, K. G., Heuser, J. E., Donzell, W. C., Ying, Y. S., Glenney, J. R., and Anderson, R. G. (1992) Caveolin, a protein component of caveolae membrane coats. *Cell* **68**, 673–682
17. Okamoto, T., Schlegel, A., Scherer, P. E., and Lisanti, M. P. (1998) Caveolins, a family of scaffolding proteins for organizing "preassembled signaling complexes" at the plasma membrane. *J. Biol. Chem.* **273**, 5419–5422
18. Isshiki, M., Ando, J., Yamamoto, K., Fujita, T., Ying, Y., and Anderson, R. G. (2002) Sites of Ca^{2+} wave initiation move with caveolae to the trailing edge of migrating cells. *J. Cell Sci.* **115**, 475–484
19. Pani, B., Ong, H. L., Brazer, S. C., Liu, X., Rauser, K., Singh, B. B., *et al.* (2009) Activation of TRPC1 by STIM1 in ER-PM microdomains involves release of the channel from its scaffold caveolin-1. *Proc. Natl. Acad. Sci. U. S. A.* **106**, 20087–20092
20. Parat, M. O. (2009) The biology of caveolae: achievements and perspectives. *Int. Rev. Cell Mol. Biol.* **273**, 117–162
21. Daniel, E. E., El-Yazbi, A., and Cho, W. J. (2006) Caveolae and calcium handling, a review and a hypothesis. *J. Cell Mol. Med.* **10**, 529–544
22. Murata, T., Lin, M. I., Stan, R. V., Bauer, P. M., Yu, J., and Sessa, W. C. (2007) Genetic evidence supporting caveolae microdomain regulation of calcium entry in endothelial cells. *J. Biol. Chem.* **282**, 16631–16643
23. Stamler, J. S., and Hess, D. T. (2010) Nascent nitrosylases. *Nat. Cell Biol.* **12**, 1024–1026
24. Kozai, D., Kabasawa, Y., Ebert, M., Kiyonaka, S., Firman, Otani, Y., *et al.* (2014) Transnitrosylation directs TRPA1 selectivity in N-nitrosamine activators. *Mol. Pharmacol.* **85**, 175–185
25. Milbourne, E. A., and Bygrave, F. L. (1995) Do nitric oxide and cGMP play a role in calcium cycling? *Cell Calcium* **18**, 207–213
26. Moncada, S., Higgs, A., and Furchgott, R. (1997) International union of pharmacology nomenclature in nitric oxide Research. *Pharmacol. Rev.* **49**, 137–142
27. Feron, O., and Balligand, J. L. (2006) Caveolins and the regulation of endothelial nitric oxide synthase in the heart. *Cardiovasc. Res.* **69**, 788–797
28. Watanabe, H., Vriens, J., Prenen, J., Droogmans, G., Voets, T., and Nilius, B. (2003) Anandamide and arachidonic acid use epoxyeicosatrienoic acids to activate TRPV4 channels. *Nature* **424**, 434–438
29. Ottolini, M., Hong, K., and Sonkusare, S. K. (2019) Calcium signals that determine vascular resistance. *Wiley Interdiscip. Rev. Syst. Biol. Med.* **11**, e1448
30. Lantoine, F., Iouzalen, L., Devynck, M. A., Millanvoye-Van Brussel, E., and David-Dufilho, M. (1998) Nitric oxide production in human endothelial cells stimulated by histamine requires Ca^{2+} influx. *Biochem. J.* **330**, 695–699
31. Lin, S., Fagan, K. A., Li, K. X., Shaul, P. W., Cooper, D. M., and Rodman, D. M. (2000) Sustained endothelial nitric-oxide synthase activation requires capacitative Ca^{2+} entry. *J. Biol. Chem.* **275**, 17979–17985
32. Koyama, T., Kimura, C., Park, S. J., Oike, M., and Ito, Y. (2002) Functional implications of Ca^{2+} mobilizing properties for nitric oxide production in aortic endothelium. *Life Sci.* **72**, 511–520
33. Yao, X., and Garland, C. J. (2005) Recent developments in vascular endothelial cell transient receptor potential channels. *Circ. Res.* **97**, 853–863
34. Dawson, V. L., Dawson, T. M., London, E. D., Bredt, D. S., and Snyder, S. H. (1991) Nitric oxide mediates glutamate neurotoxicity in primary cortical cultures. *Proc. Natl. Acad. Sci. U. S. A.* **88**, 6368–6371
35. Khan, S. A., and Hare, J. M. (2003) The role of nitric oxide in the physiological regulation of Ca^{2+} cycling. *Curr. Opin. Drug Discov. Dev.* **6**, 658–666
36. Chen, J., Wang, Y., Nakajima, T., Iwasawa, K., Hikiji, H., Sunamoto, M., *et al.* (2000) Autocrine action and its underlying mechanism of nitric oxide on intracellular Ca^{2+} homeostasis in vascular endothelial cells. *J. Biol. Chem.* **275**, 28739–28749
37. Li, N., Sul, J. Y., and Haydon, P. G. (2003) A calcium-induced calcium influx factor, nitric oxide, modulates the refilling of calcium stores in astrocytes. *J. Neurosci.* **23**, 10302–10310
38. Kwan, H. Y., Huang, Y., and Yao, X. (2000) Store-operated calcium entry in vascular endothelial cells is inhibited by cGMP via a protein kinase G-dependent mechanism. *J. Biol. Chem.* **275**, 6758–6763
39. Dedkova, E. N., and Blatter, L. A. (2002) Nitric oxide inhibits capacitative Ca^{2+} entry and enhances endoplasmic reticulum Ca^{2+} uptake in bovine vascular endothelial cells. *J. Physiol.* **539**, 77–91
40. Jaffrey, S. R., Erdjument-Bromage, H., Ferris, C. D., Tempst, P., and Snyder, S. H. (2001) Protein S-nitrosylation: a physiological signal for neuronal nitric oxide. *Nat. Cell Biol.* **3**, 193–197
41. Choi, Y. B., Tenneti, L., Le, D. A., Ortiz, J., Bai, G., Chen, H. S., *et al.* (2000) Molecular basis of NMDA receptor-coupled ion channel modulation by S-nitrosylation. *Nat. Neurosci.* **3**, 15–21
42. Xu, L., Eu, J. P., Meissner, G., and Stamler, J. S. (1998) Activation of the cardiac calcium release channel (ryanodine receptor) by poly-S-nitrosylation. *Science* **279**, 234–237
43. Gonzalez, D. R., Beigi, F., Treuer, A. V., and Hare, J. M. (2007) Deficient ryanodine receptor S-nitrosylation increases sarcoplasmic reticulum calcium leak and arrhythmogenesis in cardiomyocytes. *Proc. Natl. Acad. Sci. U. S. A.* **104**, 20612–20617
44. Xu, K. Y., Huso, D. L., Dawson, T. M., Bredt, D. S., and Becker, L. C. (1999) Nitric oxide synthase in cardiac sarcoplasmic reticulum. *Proc. Natl. Acad. Sci. U. S. A.* **96**, 657–662
45. Okada, T., Shimizu, S., Wakamori, M., Maeda, A., Kurosaki, T., Takada, N., *et al.* (1998) Molecular cloning and functional characterization of a

novel receptor-activated TRP Ca²⁺ channel from mouse brain. *J. Biol. Chem.* **273**, 10279–10287

46. Yoshida, T., Inoue, R., Morii, T., Takahashi, N., Yamamoto, S., Hara, Y., *et al.* (2006) Nitric oxide activates TRP channels by cysteine S-nitrosylation. *Nat. Chem. Biol.* **2**, 596–607

47. Takahashi, N., Mizuno, Y., Kozai, D., Yamamoto, S., Kiyonaka, S., Shibata, T., *et al.* (2008) Molecular characterization of TRPA1 channel activation by cysteine-reactive inflammatory mediators. *Channels* **2**, 287–298

48. Wong, C. O., Sukumar, P., Beech, D. J., and Yao, X. (2010) Nitric oxide lacks direct effect on TRPC5 channels but suppresses endogenous TRPC5-containing channels in endothelial cells. *Pflugers Archiv.* **460**, 121–130

49. Xu, S. Z., Sukumar, P., Zeng, F., Li, J., Jairaman, A., English, A., *et al.* (2008) TRPC channel activation by extracellular thioredoxin. *Nature* **451**, 69–72

50. Diring, S., Wang, D. O., Kim, C., Kondo, M., Chen, Y., Kitagawa, S., *et al.* (2013) Localized cell stimulation by nitric oxide using a photoactive porous coordination polymer platform. *Nat. Commun.* **4**, 2684

51. Alam, M. S. (2018) Proximity ligation assay (PLA). *Curr. Protoc. Immunol.* **123**, e58

52. Feng, X., Gaeta, M. L., Madge, L. A., Yang, J. H., Bradley, J. R., and Pober, J. S. (2001) Caveolin-1 associates with TRAF2 to form a complex that is recruited to tumor necrosis factor receptors. *J. Biol. Chem.* **276**, 8341–8349

53. Sowa, G., Pypaert, M., and Sessa, W. C. (2001) Distinction between signaling mechanisms in lipid rafts vs. caveolae. *Proc. Natl. Acad. Sci. U. S. A.* **98**, 14072–14077

54. Yu, J., Bergaya, S., Murata, T., Alp, I. F., Bauer, M. P., Lin, M. I., *et al.* (2006) Direct evidence for the role of caveolin-1 and caveolae in mechanotransduction and remodeling of blood vessels. *J. Clin. Invest.* **116**, 1284–1291

55. Brazer, S. C., Singh, B. B., Liu, X., Swaim, W., and Ambudkar, I. S. (2003) Caveolin-1 contributes to assembly of store-operated Ca²⁺ influx channels by regulating plasma membrane localization of TRPC1. *J. Biol. Chem.* **278**, 27208–27215

56. Song, K., Wei, M., Guo, W., Quan, L., Kang, Y., Wu, J. X., *et al.* (2021) Structural basis for human TRPC5 channel inhibition by two distinct inhibitors. *Elife* **10**, e63429

57. Couet, J., Li, S., Okamoto, T., Ikezu, T., and Lisanti, M. P. (1997) Identification of peptide and protein ligands for the caveolin-scaffolding domain. Implications for the interaction of caveolin with caveolae-associated proteins. *J. Biol. Chem.* **272**, 6525–6533

58. Matsubara, M., Hayashi, N., Titani, K., and Taniguchi, H. (1997) Circular dichroism and ¹H NMR studies on the structures of peptides derived from the calmodulin-binding domains of inducible and endothelial nitric-oxide synthase in solution and in complex with calmodulin. Nascent alpha-helical structures are stabilized by calmodulin both in the presence and absence of Ca²⁺. *J. Biol. Chem.* **272**, 23050–23056

59. Aoyagi, M., Arvai, A. S., Tainer, J. A., and Getzoff, E. D. (2003) Structural basis for endothelial nitric oxide synthase binding to calmodulin. *EMBO J.* **22**, 766–775

60. Mori, M. X., Erickson, M. G., and Yue, D. T. (2004) Functional stoichiometry and local enrichment of calmodulin interacting with Ca²⁺ channels. *Science* **304**, 432–435

61. Jumper, J., Evans, R., Pritzel, A., Green, T., Figurnov, M., Ronneberger, O., *et al.* (2021) Highly accurate protein structure prediction with AlphaFold. *Nature* **596**, 583–589

62. Mirdita, M., Schutze, K., Moriwaki, Y., Heo, L., Ovchinnikov, S., and Steinegger, M. (2022) ColabFold: making protein folding accessible to all. *Nat. Methods* **19**, 679–682

63. Chaudhuri, P., Colles, S. M., Bhat, M., Van Wagoner, D. R., Birnbaumer, L., and Graham, L. M. (2008) Elucidation of a TRPC6-TRPC5 channel cascade that restricts endothelial cell movement. *Mol. Biol. Cell* **19**, 3203–3211

64. Zhou, Y., Castonguay, P., Sidhom, E. H., Clark, A. R., Dvela-Levitt, M., Kim, S., *et al.* (2017) A small-molecule inhibitor of TRPC5 ion channels suppresses progressive kidney disease in animal models. *Science* **358**, 1332–1336

65. Broker-Lai, J., Kollewe, A., Schindeldecker, B., Pohle, J., Nguyen Chi, V., Mathar, I., *et al.* (2017) Heteromeric channels formed by TRPC1, TRPC4 and TRPC5 define hippocampal synaptic transmission and working memory. *EMBO J.* **36**, 2770–2789

66. Hofmann, T., Schaefer, M., Schultz, G., and Gudermann, T. (2002) Subunit composition of mammalian transient receptor potential channels in living cells. *Proc. Natl. Acad. Sci. U. S. A.* **99**, 7461–7466

67. Minshall, R. D., Sessa, W. C., Stan, R. V., Anderson, R. G., and Malik, A. B. (2003) Caveolin regulation of endothelial function. *Am. J. Physiol. Lung Cell Mol. Physiol.* **285**, L1179–L1183

68. Mathew, R. (2021) Critical role of caveolin-1 loss/dysfunction in pulmonary hypertension. *Med. Sci. (Basel)* **9**, 58

69. Goligorsky, M. S., Li, H., Brodsky, S., and Chen, J. (2002) Relationships between caveolae and eNOS: everything in proximity and the proximity of everything. *Am. J. Physiol. Ren. Physiol.* **283**, F1–F10

70. Wang, L., Karlsson, L., Moses, S., Hultgardh-Nilsson, A., Andersson, M., Borna, C., *et al.* (2002) P2 receptor expression profiles in human vascular smooth muscle and endothelial cells. *J. Cardiovasc. Pharmacol.* **40**, 841–853

71. Goedicke-Fritz, S., Kaistha, A., Kacik, M., Markert, S., Hofmeister, A., Busch, C., *et al.* (2015) Evidence for functional and dynamic microcompartmentation of Cav-1/TRPV4/K_Ca in caveolae of endothelial cells. *Eur. J. Cell Biol.* **94**, 391–400

72. Goel, M., Sinkins, W. G., and Schilling, W. P. (2002) Selective association of TRPC channel subunits in rat brain synaptosomes. *J. Biol. Chem.* **277**, 48303–48310

73. Kollewe, A., Schwarz, Y., Oleinikov, K., Raza, A., Haupt, A., Wartenberg, P., *et al.* (2022) Subunit composition, molecular environment, and activation of native TRPC channels encoded by their interactomes. *Neuron* **110**, 4162–4175.e4167

74. Chen, Z., S, D. S. O., Zimnicka, A. M., Jiang, Y., Sharma, T., Chen, S., *et al.* (2018) Reciprocal regulation of eNOS and caveolin-1 functions in endothelial cells. *Mol. Biol. Cell* **29**, 1190–1202

75. Singh, B. B., Liu, X., Tang, J., Zhu, M. X., and Ambudkar, I. S. (2002) Calmodulin regulates Ca²⁺-dependent feedback inhibition of store-operated Ca²⁺ influx by interaction with a site in the C terminus of TrpC1. *Mol. Cell* **9**, 739–750

76. Yokomori, H., Oda, M., Yoshimura, K., Nomura, M., Wakabayashi, G., Kitajima, M., *et al.* (2003) Elevated expression of caveolin-1 at protein and mRNA level in human cirrhotic liver: relation with nitric oxide. *J. Gastroenterol.* **38**, 854–860

77. Machleidt, T., Li, W. P., Liu, P., and Anderson, R. G. (2000) Multiple domains in caveolin-1 control its intracellular traffic. *J. Cell Biol.* **148**, 17–28

78. Strubing, C., Krapivinsky, G., Krapivinsky, L., and Clapham, D. E. (2001) TRPC1 and TRPC5 form a novel cation channel in mammalian brain. *Neuron* **29**, 645–655

79. Sundivakkam, P. C., Kwiatek, A. M., Sharma, T. T., Minshall, R. D., Malik, A. B., and Tiruppathi, C. (2009) Caveolin-1 scaffold domain interacts with TRPC1 and IP₃R3 to regulate Ca²⁺ store release-induced Ca²⁺ entry in endothelial cells. *Am. J. Physiol. Cell Physiol.* **296**, C403–C413

80. Brenman, J. E., Chao, D. S., Gee, S. H., McGee, A. W., Craven, S. E., Santillano, D. R., *et al.* (1996) Interaction of nitric oxide synthase with the postsynaptic density protein PSD-95 and alpha1-syntrophin mediated by PDZ domains. *Cell* **84**, 757–767

81. Nakamura, T., and Lipton, S. A. (2013) Emerging role of protein-protein transnitrosylation in cell signaling pathways. *Antioxid. Redox Signal.* **18**, 239–249

82. Ray, F. R., Huang, W., Slater, M., and Barden, J. A. (2002) Purinergic receptor distribution in endothelial cells in blood vessels: a basis for selection of coronary artery grafts. *Atherosclerosis* **162**, 55–61

83. Fulton, D., Fontana, J., Sowa, G., Gratton, J. P., Lin, M., Li, K. X., *et al.* (2002) Localization of endothelial nitric-oxide synthase phosphorylated on serine 1179 and nitric oxide in Golgi and plasma membrane defines the existence of two pools of active enzyme. *J. Biol. Chem.* **277**, 4277–4284

84. Freichel, M., Suh, S. H., Pfeifer, A., Schweig, U., Trost, C., Weissgerber, P., *et al.* (2001) Lack of an endothelial store-operated Ca^{2+} current impairs agonist-dependent vasorelaxation in TRP4$^{-/-}$ mice. *Nat. Cell Biol.* **3**, 121–127

85. Gomis, A., Soriano, S., Belmonte, C., and Viana, F. (2008) Hypoosmotic- and pressure-induced membrane stretch activate TRPC5 channels. *J. Physiol.* **586**, 5633–5649

86. Mori, M. X., Imai, Y., Itsuki, K., and Inoue, R. (2011) Quantitative measurement of Ca^{2+}-dependent calmodulin-target binding by Fura-2 and CFP and YFP FRET imaging in living cells. *Biochemistry* **50**, 4685–4696

87. Takahashi, N., Kuwaki, T., Kiyonaka, S., Numata, T., Kozai, D., Mizuno, Y., *et al.* (2011) TRPA1 underlies a sensing mechanism for O_2. *Nat. Chem. Biol.* **7**, 701–711